Investigating Bismuth-based Perovskite Solar Cells

A thesis submitted to the faculty of The University of Minnesota by

Emmannuel Khora

in partial fulfillment of the requirements for the degree of Master of Science
in Chemical Engineering

Advisor: Dr Zhihua Xu

December 2019

Copyright 2019
Emmannuel Khora

Contents

Acknowledgement

Many thanks to God almighty, by whose grace and mercy I would remain strong and focused. It is only by God's grace that He gave me such knowledge and wisdom to complete my thesis strong.

I'm grateful to my advisor Dr. Zhihua Xu. Your patience and guidance were very crucial for the development of my thesis. I appreciate a lot for all the help and motivation to achieve the same.

A special gratitude to Dr. Michael Rother and Dr. Stanley Burns who served as my committee members. You both provided me valuable guidance and suggestions at the time when you both were busy.

With a special mention to River Church Duluth family who always stood in my difficult times. I moved to various homes in these two years and it was always the River Church who made it smooth and easy.

I appreciate the help from Dr. Tsutomu Shimotori with X-ray diffraction training and giving me the opportunity to test the samples at RIL.

And finally, I am grateful of all the students and staffs with whom I worked for these two years. All of the them kept me motivated and helped me to be focused.

Abstract

Solar Cells are one of the most prominent alternatives for fossil fuels. In recent years perovskite solar cells has gained a lot of attention due to its high photovoltaic performance, low cost and the ease of fabrication. However, one of the drawbacks of perovskite solar cells is the toxic constituent element lead (Pb) in the perovskite structure in the form of ABX_3, e.g. methylammonium lead iodide ($CH_3NH_3PbI_3$). To find an alternative to replace lead (Pb) without changing the established perovskite structure, bismuth (Bi) was investigated on the basis of split-ion approach where a three-layer (Bi_2Te_2, BiI_3, and CH_3NH_3I) deposition process was formulated to fabricate perovskite structure in the form of $CH_3NH_3BiTeI_2$. Our novelty resides in a unified approach of studying bismuth telluride as a possible compound which would react with bismuth iodide and then having a three-layer deposition method with methylammonium iodide to form a single crystal structure. The solar cells based on the novel lead-free perovskite material have a power conversion efficiency of 0.06%, open-circuit voltage of 0.46 V and current density of 0.38 mA/cm^2. Absorption spectrum were used to identify the optimal annealing temperatures to form the perovskite structure. X-ray diffraction showed few peaks matching to the lead-based perovskite $CH_3NH_3PbI_3$, which suggests the tetragonal perovskite structure was partially formed. The compositional gradient existing in the thermal evaporated Bi_2Te_3 thin film might be the major culprit leading to the incomplete formation of perovskite structure.

List of Figures

List of Tables

Nomenclature

A	Absorbance
c	velocity of light
E	charge carrier energy level
E_g	Bandgap
E_c	conduction band energy level
E_F	Fermi energy level
$f(E)$	Fermi Dirac distribution function
FF	Fill factor
h	Plank's constant
i	Intensity of transmitted light
i_0	Intensity of incident light
I	Current
I_L	Photocurrent
I_F	Forward bias current
I_m	Maximum current
I_{sc}	Short circuit current
J_{sh}	Current density
k	Boltzmann's constant
L	Path-length of the light
m^*	Effective mass
n_0	Electron concentration
N_c	density of states in conduction band
P	Power
P_m	Maximum power
P_{in}	Power input
P_{out}	Power output
V	Voltage
V_m	Maximum voltage

V_{oc}	Open circuit voltage
η	Efficiency
ν	Photon's frequency
λ	Wavelength
α	Absorption coefficient

CHAPTER 1 Introduction

1.1 Renewable and non-renewable sources of energy

Energy is the foundation of the human civilization whether it is from renewable or non-renewable sources of energy. After the first Industrial Revolution there has been a greater consumption of energy along with its increasing demand. It has been the driving force for technological advancement and innovation, which has transformed the human lifestyle dramatically. This has become evident after World War II, which increased the consumption of energy industrially and transition of countries into an industrialized, urbanized and technological boom. According to BP's report in 2019[1] from 1965 to 2018 the world energy consumption has increased from 43 petawatt-hour (PWh) to 161 PWh.

The consumption of global energy has been increasing significantly since 2010 and is almost the double in the 10-year average. The demand for all fuels increased but the growth of gas and renewables increased in greater measure accounting for 43% and 18% respectively in the global growth. The countries which are at the top in the energy consumption are China, US and India which contributed to two-thirds of the rest of the world. The demand and consumption are expected to increase a lot and at a faster rate in near future as there are many developing countries and we all are striving for better human life. [1]

Although there is a significant increase in the renewable sources of energy, it is still only 4% of the total energy consumed. Fossil fuels in terms of oil, coal, and natural gas are still the major energy consumption sector. The production and consumption of fossil fuels release emissions and dust to the environment. These emissions are a major factor of

climate change and global warming, causing a greater damage to the ecosystem and thereby the safety of mankind.

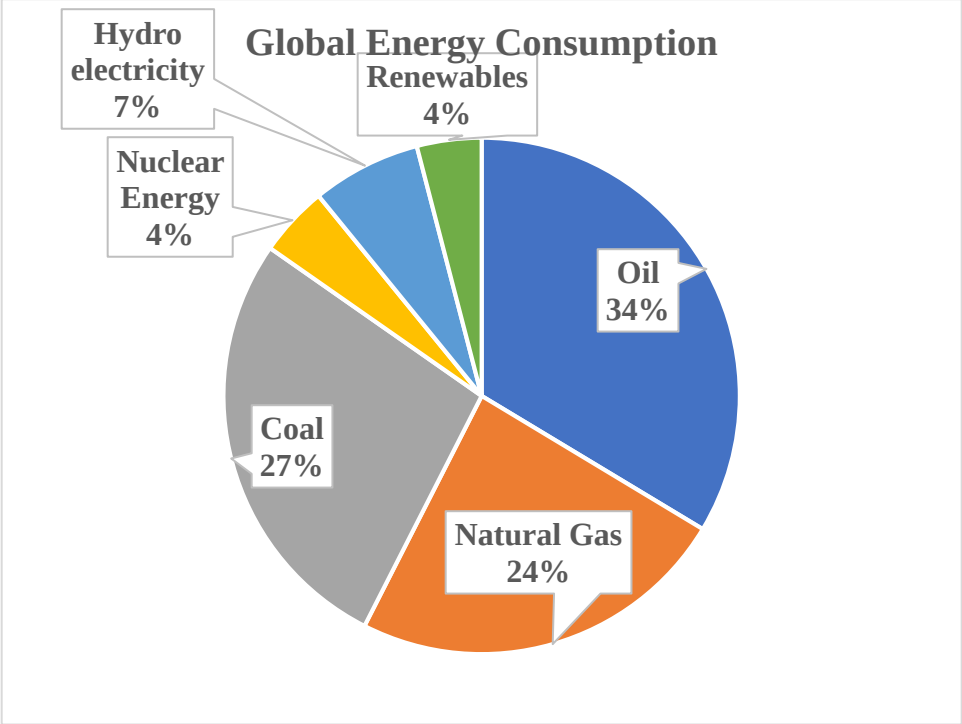

Figure 1: Global Energy Consumption [54]

As a way forward with the global consumption of energy especially in the sector of fossil fuels, there is a greater need of encouragement and advancement in the use of renewable sources of energy. In fact, the theoretical potential of solar energy is 89,300 terawatt-hour (TWh) which represents more energy striking on earth's surface in one and a half hour than the worldwide energy consumption in the year 2001 from all sources combined.

However, this is not the extractable solar energy, technical extractable potential of solar energy is around 15,600 TW_ch (where the subscript c represents the equivalent chemical fuel) which is also a huge potential. [2] Even with this, the harvestable solar energy is

reduced to few thousand-terawatts due to geographical accessibility and current technology. This few harvestable energies are nevertheless a huge amount of energy which can meet a large amount of global energy consumption.[3]

The US Energy Information Administration (EIA) in March 2018, published its report which was taken over in a period of 30 years of different energy sources, revealed the data in the following picture:

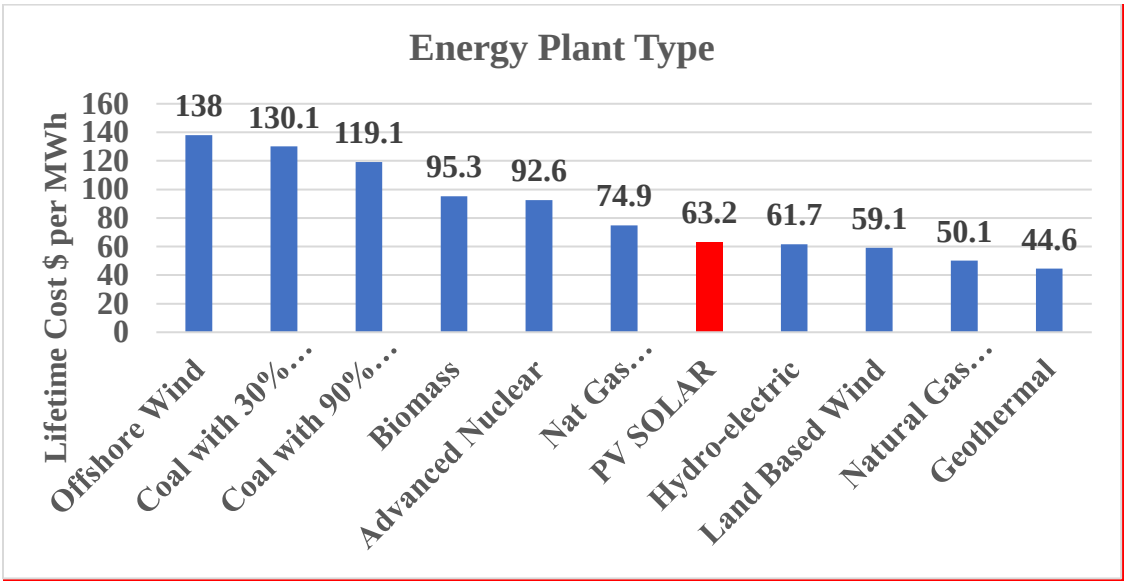

Figure 2: Energy plant type

As we see, solar PV is about $63.20 per MWh which is much cheaper than coal. Geothermal, hydro-electric and biomass aren't the mainstream electricity producing sector. Therefore, as far as electrical facilities are concerned, the main contributors for the generation of electricity is likely to be natural gas, land-based wind and solar. Wind is limited to the flow of air within an area and there should be a flowrate of more than 20 miles per hour and there are not many places where the average wind flow is more than 20

miles per hour every day. When we compare this with the solar energy, sun shines almost everywhere, and it makes the best candidate for the source of energy[1].

1.2 Photovoltaic Solar Cells

There are various ways to extract or harvest solar energy, some of them are photovoltaics (PV), solar thermal electricity and solar heating and cooling, which are well established technologies. Solar photovoltaics (PV) system converts the solar energy directly into electricity and has a wide range of applications. It can be either manufactured in large scale industries leading into very good economics or can be scaled down to product-based specific requirements like photovoltaics for calculators or smaller appliances. On the other hand, it can be manufactured for a high-power generation utility scale facility. The cumulative energy harvested by PV in the year 2017 was almost 398 gigawatt (GW) and generated about 460 terawatt-hour (TWh), representing 2% of the total global power output. The utility-based projects account for almost 60% of the total PV installed application. The International Energy Agency estimated that by the year 2023, solar photovoltaics would lead the generation of electricity in the renewable sources of energy. The cost of PV was not the same from the very beginning, in fact the cost of manufacturing was really high, which was around $100 per watt in 1970s. This has been gradually decreasing due to the advancement in research and technology in the field of PV and now is around $0.47 per watt in 2018.[2]

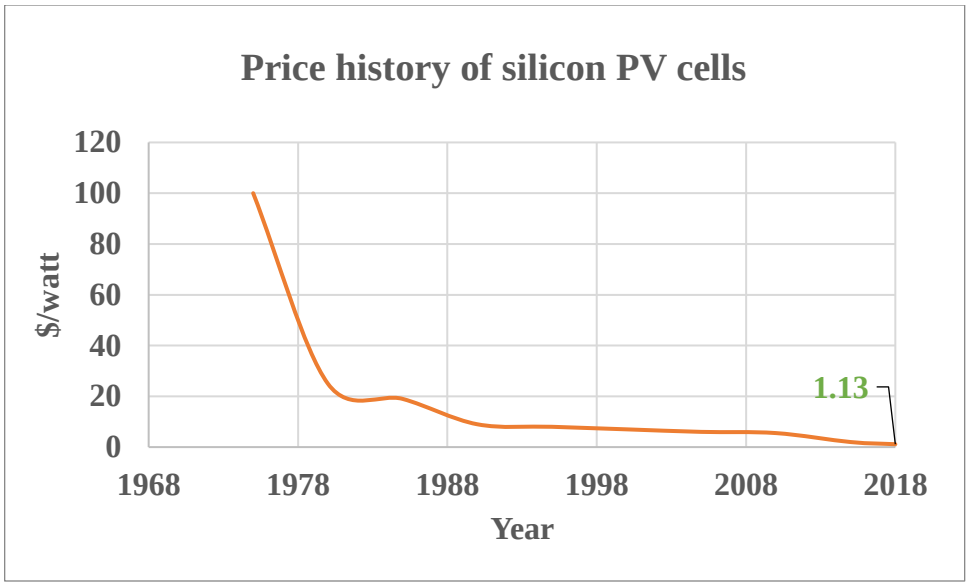

Figure 3: Decreasing cost of solar cell[3]

This low cost is only for the laboratory research, whereas the actual cost in US for complete solar cell fabrication and installation is around $1.13 per watt. [3]

The first photovoltaic characteristic was found in the element selenium by 19-year-old *Edmund Becquerel* in 1839. [4]After that, silicon has been used as the dominant semiconductor element with a power conversion efficiency of 25%. In recent years semiconducting perovskite materials have been demonstrating a lot of promising properties, like a power conversion efficiency of 23.7% within a research period of less than 20 years. [5]

1.3 Working principal of semiconductor photovoltaics

Sun light contains photons with a wide range of wavelength from 200 nm to 2600 nm. When semiconductors are exposed to sun light, the phonons from the solar spectrum excite the electrons in semiconductors to a broader range of energy states in the conduction band. These electrons collide into the semiconductor atoms causing them to transfer their excess energy to the other atoms in the semiconductor. The electrons which are transferred usually settle near the conduction band, this process is known as thermalization. It happens so fast that most of the electrons relax at the edge of the conduction band before reaching a contact and the energy is lost in the form of heat. This thermalization process also takes place in the valence band, when the electrons are excited in the conduction band, they leave the hole behind in the valence band in the wide range of energy. These holes are being filled by the electrons from the higher valence band until the holes settle near the valence band edge.[6]

The electrons on the edge of the conduction band do not stay there forever. They fill up the holes and this process is known as recombination. Since this process takes a long time (in terms of milliseconds), many of the electrons reach the metal contact and deliver power to the circuit. Thus, the probability of recombination depends on the density of holes times density of electrons: $p*n$. This implies that the recombination rate is dependent on the less abundant carriers or the minority carriers. As the recombination rate is dependent on $p*n$, the voltage V also plays an important role in the p and n carriers. The minority carrier

density increases exponentially and so does the recombination rate and the current through the diode.

The energy band gap (Eg) of semiconductors is generally below 5 eV, whereas insulators are in the range of 5-15 eV. Metals on the other hand have a different type of band structure, where the valance and conduction bands overlap each other.

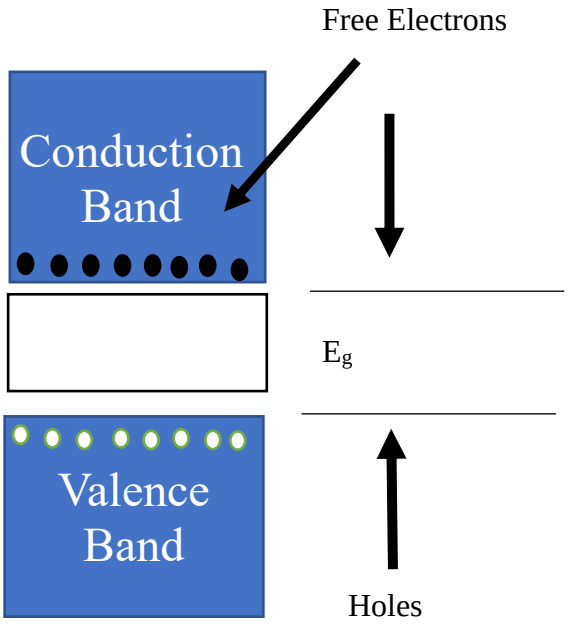

Figure 4: Energy band diagram of a semiconductor[7]

To understand the working mechanism of a solar cell, let us first consider *p-n* junction solar cell. The net current in a semiconductor is given by

$$I = I_L - I_F = I_L - I_S \left[e^{\left(\frac{eV}{kT}\right)} - 1 \right] \qquad (1)$$

Where I_L is the photocurrent, I_F is the forward bias current and they both are in opposite direction. I_S is the reverse saturation current.

k is the Boltzmann's constant in eV K^{-1}

T is the temperature in Kelvin

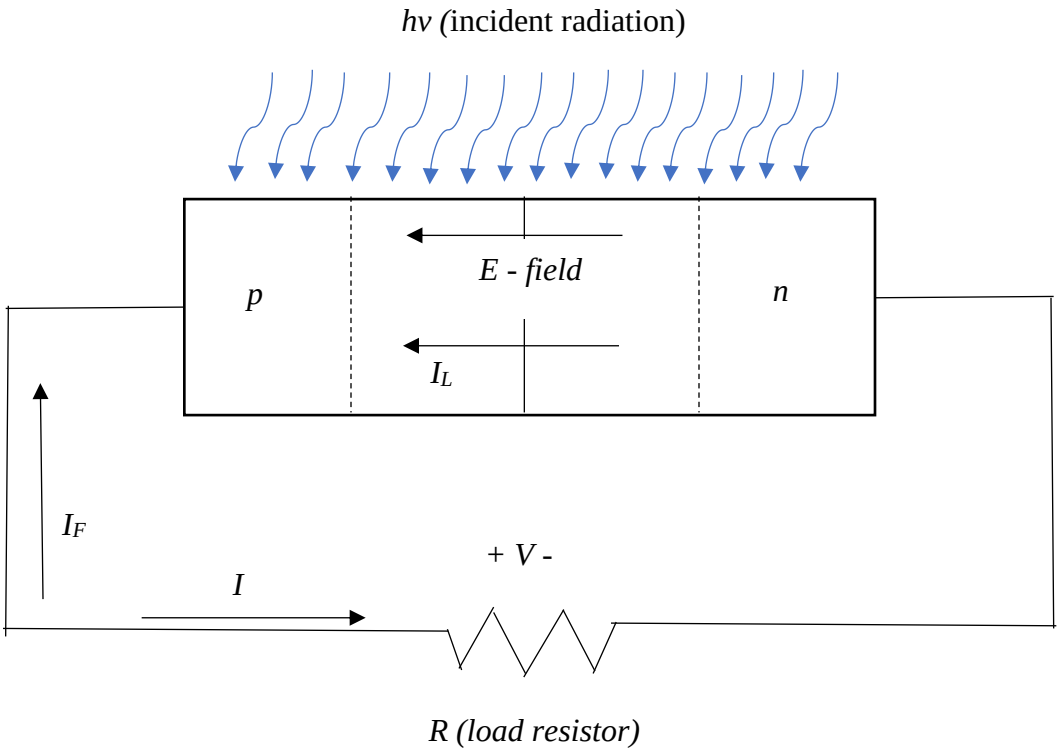

Figure 5: Illuminated p-n junction diode [8]

Where I is net current in *p-n* junction in Ampere

I_L is photocurrent in Ampere

I_F is forward bias current in Ampere

E is the electric field in Newton

hv is incident photon energy in eV

The two important characteristics on the *I-V* curve are the short-circuit current, I_{SC}, and the open-circuit voltage, V_{OC} (in Volts). Under short-circuit conditions, resistance $(R)=0$ ohm, equation (1) becomes

$$I = I_L = I_{SC} \qquad (2)$$

Whereas on the other hand, if $R=\infty$, the circuit becomes open-circuit. When there is no current, $I=0$ ohm, the above equation converts into

$$V_{OC} = kT/e \ ln \ (1 + I_L/I_S) \quad (3)$$

Power (P) is given by the equation:

$$P = IV \quad (4)$$

where power is in watts

Substituting equation [3] in [4] we get

$$P = I_L V - I_S[exp(eV/kT) - 1]V \quad (5)$$

The maximum power is given by

$$P_m = I_m V_m \quad (6)$$

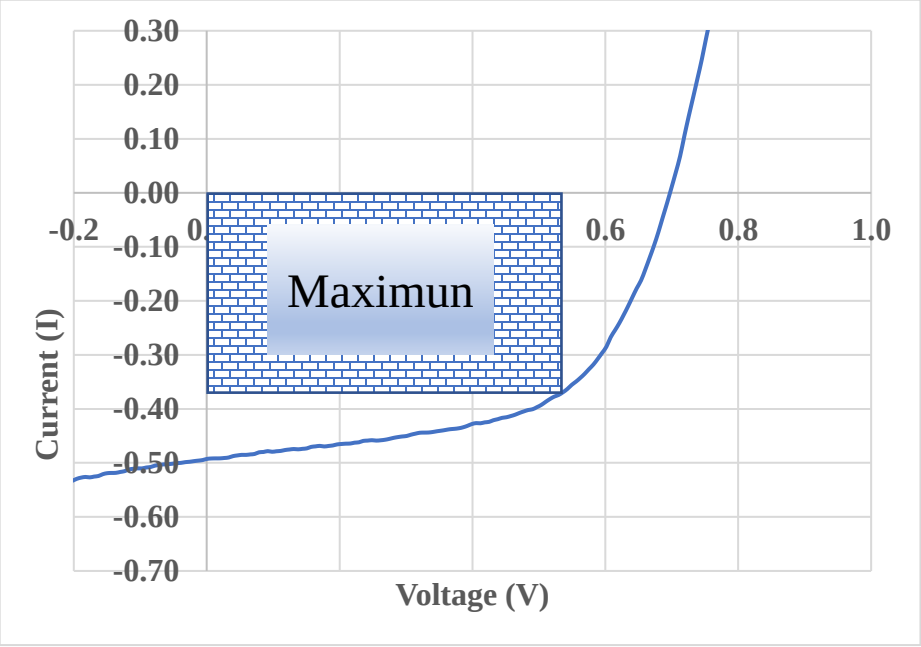

Figure 6: I-V characteristic curve of a perovskite solar cell under illumination[8]

One of the most important parameters to study the performance of a solar cell is the power conversion efficiency (PCE). [9]The conversion efficiency of a solar cell is the ratio of the output electrical power to the input light power. Assuming maximum power output, we can write efficiency, η,

$$\eta = P_{out}/P_{in} \text{ x } 100\% \quad (7)$$

$$P_{out} = P_{max} = I_m V_m \quad (8)$$

$$\eta = I_m V_m / P_{in} \text{ x } 100\% \quad (9)$$

Another important parameter which contributes a lot in the power conversion efficiency is the Fill Factor, abbreviated as "FF", which is the conjunction of short-circuit current and open-circuit voltage. It is defined as the ratio of the maximum power from solar cell (which is $V_m I_m$) to the product of V_{oc} and I_{sc}.

$$FF = I_m V_m / I_{sc} V_{oc} \quad (10)$$

Combining the above equations, we get the efficiency as

$$\eta = FF\ I_{sc} V_{oc} / P_{in} \quad (11)$$

It is clear from the above equation that we need to maximize the fill factor, short-circuit current and open-circuit voltage to get the maximum efficiency.

1.4 Optical Absorption

The energy of a photon *E*, is related to the frequency, *v* in second^{-1}, by the equation

$$E = hv \qquad (12)$$

Where *h* is the Planck's constant in electronVolt second. The frequency in-turn is related to the wavelength, λ in μm, through the equation

$$v = c/\lambda \qquad (13)$$

where c is the velocity of light in $\mu m/s$. This can be simplified as

$$\lambda = c/v = hc/E = 1.24/E\ \mu m \qquad (14)$$

the value of E is in eV

When photons are incident on the semiconductor, they interact in various ways including the interaction with donors, acceptors, defects or lattice atoms. Photons can exchange their energy from the valence electrons and can help them jump from the valence band to the conduction band, thereby being responsible for the generation of an electron-hole pair.[10]

To understand more about absorption, we need to study the Beer Lambert law, which plays an important role in estimating the parameters of absorption. It is explained by the following diagram.

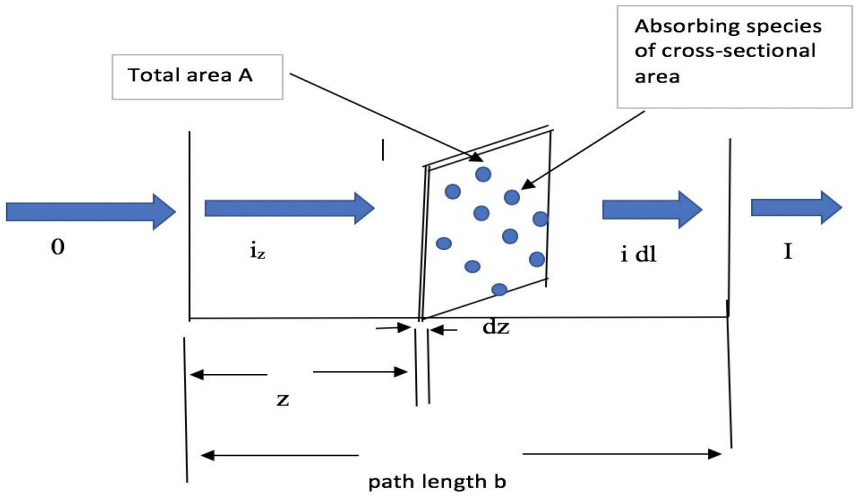

Figure 7: Explaining Beer Lambert law

$$i = i_0 e^{-\alpha L} \quad (15)$$

$$i/i_0 = e^{-\alpha L} \quad (16)$$

Taking log on both sides, we get:

$$\log\left(\frac{io}{i}\right) = \alpha L \log(e) \quad (17)$$

Absorbance of a material can be defined as the logarithmic ratio of the intensity of incident light (i_0) to that of the intensity of the transmitted light (i). This is given by:

$$A = \log(\frac{io}{i}) \quad (18)$$

Substitution the value of A in equation (17) we get:

α = A / (0.4343L) in nm^{-1}

L = path-length of the light in nm

Intensities of the light is in W/nm^2

The frequency of the photons and the energy band gap of a semiconductor determines the interaction of light and semiconductor. If the energy of a photon is less than E_g then the

photon travels through the semiconductor and it acts as a transparent material. If the energy of the photon is greater than E_g of the semiconductor then the photon excites the electron in the valence band to jump into the conduction band and dissipates heat.

On the other hand, if E_g is equal to $h\nu$, then the electron is just reaching the conduction band and there is not heat dissipation.

Absorbance is also given by the logarithmic ratio of the radiant flux received by transmitted. The absorption strength depends on the photon energy and the band gap as shown in the equation:

$$(\alpha h\nu)^{1/n} = a(h\nu - E_g) \qquad (19)$$

Where h = Plank's constant in eV s

ν = photon's frequency in s^{-1}

α = absorption coefficient in nm^{-1}

E_g = Band gap in eV

a = proportionality constant in nm^{-1}

The exponential value denotes the nature of electronic transition, which has 4 different types of electronic transition. They are:

a. Direct allowed transitions n= ½
b. Direct forbidden transitions n=3/2
c. Indirect allowed transitions n=2
d. Indirect forbidden transitions n=3

Semiconductors are always allowed transitions; some are direct, and some are indirect. Direct transitions are those where the energy changes i.e. it either increases or decreases

but the momentum is conserved, whereas indirect transitions are those where both energy and momentum (wave-vector) changes. If the momentum matrix element is different from zero then it is an allowed transition, whereas if it equals to zero then it's a forbidden transition. Our samples are direct allowed transitions; therefore, we use the exponential value n = 1/2 in equation (19) to form the Tauc plot which helps us to know the energy band gap of the film.

1.5 Perovskite structure in the form of ABX_3

The term "perovskite" is interchangeable with "perovskite structure". Technically, a perovskite is a type of mineral that was found in the Ural Mountains and named after *Lev Perovskite,* who was the founder of the Russian Geographical Society. A perovskite structure is any compound that has the same structure as the perovskite mineral. A true perovskite (mineral) is composed of calcium, titanium and oxygen in the form of $CaTiO_3$, whereas a perovskite structure is the one which has the generic formula of ABX_3 and the same crystallographic structure as perovskite. With crystallography, it can be represented in various ways, but the best way to represent is the cubic structure. The first perovskite-structured hybrid halide compound was reported by Weber in 1978, but it emerged on the most trending tops in the field of photovoltaics only after the seminal work by *Akihiro Kojima* at The University of Tokyo in 2008 with $CH_3NH_3PbI_3$ yielding a power conversion efficiency of 3.8%. [11]

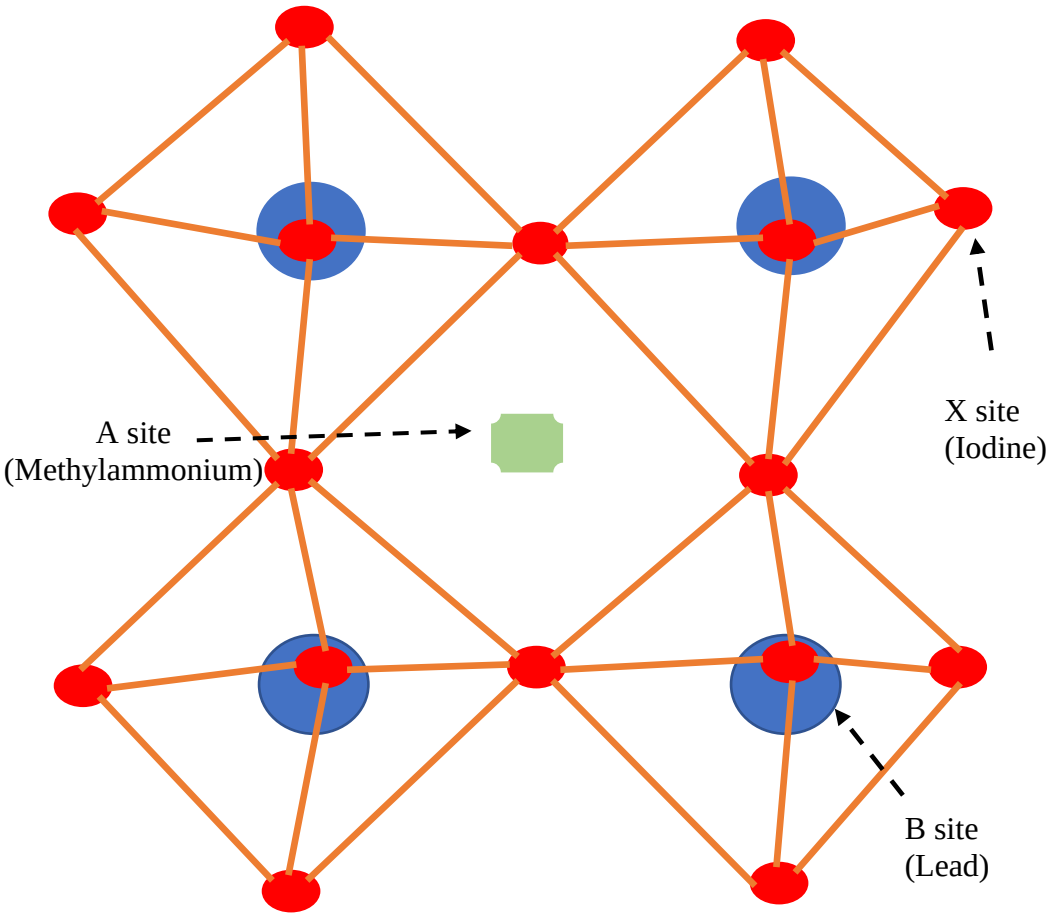

Figure 8: Perovskite structure in the form of ABX_3 [12]

In a perovskite structure, A and B are the cations and X is the anion, which bonds to both. Cation A is much larger than the cation B. In each functional unit, cation A is surrounded by eight B cations in the form of a cube, whereas cation B is surrounded by six X anions

in the form of octahedra. For example, the most widely used perovskite in solar cells is methylammonium lead iodide ($MAPbI_3$, or $CH_3NH_3PbI_3$).[13]

1.6 Lead based Perovskite Solar cells

The first perovskite in the form of organic-inorganic hybrid halide was used in the form of liquid-electrolyte-based dye-sensitized in 2006[14] . It is the discovery of $MAPbI_3$ which opened the flood gates in the research of perovskite, and a wide range of research avenue was established in the field of perovskite solar cells. At around 2009, there was $MAPbI_3$ and $MAPbBr_3$ which came into picture as a perovskite structure with a power conversion efficiency of around 3-4%, eventually in subsequent years, around the year 2011 the power conversion efficiency doubled and it kept on increasing until 2016 when the National Renewable Energy Laboratory released its best efficiency data as 22.1%. Up-to-date, photovoltaic devices based on $MAPbI_3$ are still the most efficient and most widely studied perovskite solar cells. [15]

In-spite of this breakthrough in the power conversion efficiency and other properties, it has some draw backs which include the stability of the solar cell, the discrepancy in reverse and forward scan of current-voltage (*I-V)* curves (also called as *I-V* hysteresis). Nonetheless, the toxicity of lead in the perovskite structure is one of the most critical constraints for the commercialization of this promising solar energy technology.

1.6.1 Need for the replacement of Lead

Lead-based perovskites cannot be commercialized considering its harmful toxic effects on the environment and mankind. The research on replacement of lead (Pb) from the halide perovskite solar cells have already started since the first demonstration of the photovoltaics character of $MAPbI_3$. [6] A detailed assessment of the impact on the use of toxic element lead on perovskite solar cell is premature at this stage. But it is evident from the regulations being imposed by many of the countries and societies that it cannot be used for commercialization. One of the regulations which is adhered by the European Union is from the Reduction of Hazardous Substances (RoHS), which regulates "Directive on the restriction of the use of certain hazardous substances in electrical and electronic equipment" in 2003 and subsequently in 2011 which is also known as "lead-free directive". According to RoHS, the standard to maintain heavy metals is; its concentration in photovoltaics or electron devices should be less than 0.1% in weight. Unfortunately, the halide perovskite solar cells researched are more that 10% concentration in weight.

Although the restrictions set by RoHS have certain exceptions, like there is exemption for high content of cadmium in cadmium telluride for European energy market. However, these exemptions cannot be replicated for lead in the halide perovskite photovoltaics as it has a higher possibility of getting dissolved in water, which in turn can easily get into our food chain. There have been intensive studies of harmful effects of lead into our food chain, especially for children. [6]

Many lead-free perovskite compositions are been tried and tested following the discovery of the great potential in the lead-based perovskite photovoltaics. In the lead-based

perovskite structure of ABX_3, Pb^{+2} electronic configuration plays a very vital role. Therefore, research has been keenly focused in replacing lead with +2 charge i.e. isoelectronic s^2p^2 elements within group IV.[17] To attain a +2 charge in the electronic configuration it has to give away p electrons and retain the s electrons to form a stable structure. To replace lead (Pb) the best choices would be group IV elements i.e. carbon (C), silicon (Si), germanium (Ge) and tin (Sn). However, tin and germanium would be the best choices since they are near lead in the periodic table and can share same characteristics, but unfortunately, they are more stable in +4 oxidation state. Attempts for a lead-free perovskite with tin and germanium in the form of ABX_3 resulted in products with issues in stability. Also, the power conversion efficiency for Sn based perovskite was only 8% as reported by Zhao et al.[18] with a composition of $(FA)_{0.75}(MA)_{0.25}SnI_3$. Film morphology and device fabrication atmosphere during its fabrication played a very vital role in forming the structure, thereby giving a very high performing device. [19][20]

CHAPTER 2 Experimental Methods

2.1 Fabrication of perovskite solar cells

The schematic structure of perovskite solar cell is shown in *figure 9*. The fabrication starts with a cleaned glass substrate coated with fluorine doped indium tin oxide (FTO), serving as cathode contact, followed by coating of a compact titanium oxide (TiO_2) thin film and a mesoporous TiO_2 layer, which act as electron transporting layer (ETL). Then a perovskite thin film, acting as light-absorbing material, is deposited on top of ETL. A hole transporting layer (HTL) is then coated on top of the perovskite, followed by vacuum-deposition of a metal film as anode contact.

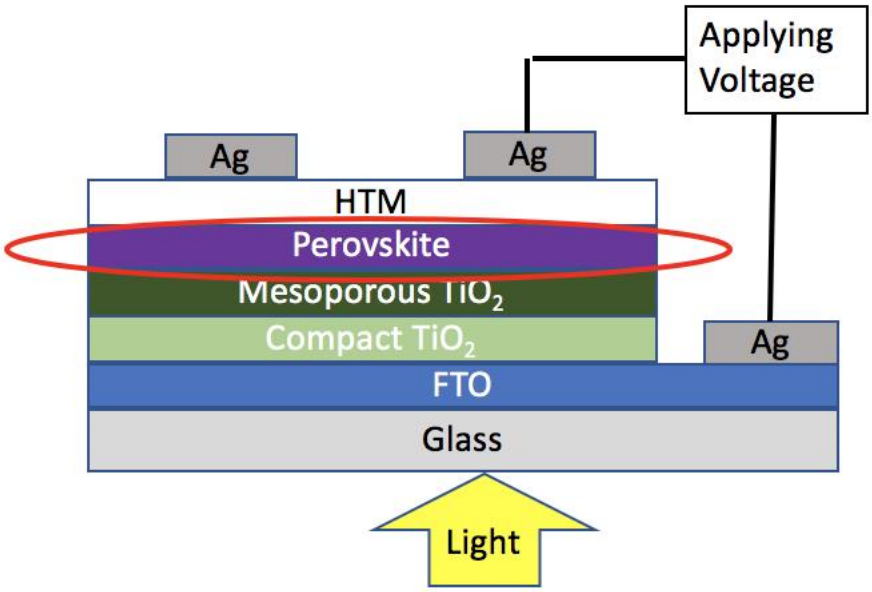

Figure 9: Schematic diagram of different layers in a Perovskite solar cell

2.1.1 Substrate preparation

A 1.5 cm x 1.5 cm x 1 mm thick glass square coated with 1.5 cm x 1.0 cm fluorine doped indium tin oxide (FTO) with a resistivity of 18 Ω-cm^2 was rinsed with deionized water and

then with isopropyl alcohol. The samples were then cleaned with deionized water solution containing 1 mass % detergent and 5 mass % ethanol for 5 minutes in a 500 mL beaker. Samples were then transferred into a clean beaker of DI water and ultrasonic cleaned for an additional 3 minutes. Then rinsed with additional DI water, air dried and finally cleaned with an UV-Ozone generator for 30 minutes.

2.1.2 Electron transporting layer (TiO_2)

1.0 M $TiCl_4$ solution was prepared by mixing 1.23 mL of 99% $TiCl_4$ (Sigma-Aldrich) in 10 mL of ice. The ice+$TiCl_4$ solution was mixed until melted and the solution was allowed to reach room temperature. Samples were then spin coated with 1.0 M $TiCl_4$ solution at 3000 rpm at 1000 rpm/second acceleration for 30 seconds using Best Tools Smart Coater 100. The thin film of $TiCl_4$ over the samples were then annealed at 550^o C for 15 minutes to get a compact layer of TiO_2.[21] Samples were allowed time heat up and cool down over the hot plate to avoid induced thermal stressed due to rapid expansion or contraction.

The mesoporous titanium dioxide solution was prepared with 100 mg of DYESOL 18 NR-T TiO_2 paste with 0.4 mL of terpineol (Sigma-Aldrich, anhydrous) and 0.2 mL of ethanol (Sigma-Aldrich, >99.99%). All these were mixed in a vibrator mixture for 15 minutes. The mesoporous solution of TiO_2 was then spin coated over the samples at 4000 rpm at 1000 rpm/second acceleration for 60 seconds. The coated samples were then annealed at 550^o C for 1 hour allowing them to heat and cool down on the hot plate. This completes the ETM layer.[22]

2.1.3 Perovskite Layer

Here we describe the fabrication of three different types of perovskite layers

a. Lead-based perovskite

Lead-based perovskite layers are fabricated by mixing lead iodide (PbI_2) (Sigma-Aldrich, 99%) and methylammonium iodide (CH_3NH_3I) (Sigma-Aldrich, 99%) in equimolar concentration and dissolved in 3:7 volume ratio of Dimethyl Sulfoxide (DSMO) to γ-butyrolactone (GBA) (Sigma-Aldrich, 99%). This precursor solution was well mixed in a vibrator mixture. Then it was coated on top of electron transport layer at 4000 rpm at 1000 rpm/second acceleration for 60 seconds and annealing the sample at 100 ^{0}C for 1-5 hours in a nitrogen flow glove box so as to avoid any oxidation reaction.

b. Bismuth-based perovskite

In bismuth-based perovskite solar cell, the perovskite layer is coated in two different methods: One-step and two-step method.

In **two-step method**, 200 mg of bismuth iodide (BiI_3) (Sigma-Aldrich, 99%) is dissolved in 0.5 ml of dimethylformamide (DMF) as solvent with a volume ratio of 7/3, which was filtered through a 0.45-micron PTFE syringe filter to avoid the undissolved particles. This precursor solution was coated over the electron transport layer at 4000 rpm at 1000 rpm/second for 40 seconds. This substrate was annealed at 120 ^{0}C in nitrogen flow for 1-5 hours. After that, methylammonium iodide (Sigma-Aldrich, 99%), precursor solution was made by mixing with iso-propyl alcohol at a concentration of 10 mg/ml. It was coated on top of bismuth iodide at 4000 rpm at 1000 rpm/second for 40 seconds and then the sample was annealed at 110 ^{0}C for 1-5 hours in a nitrogen flow glove box.

In **one-step method,** the precursor solution for perovskite is prepared by mixing methylammonium iodide and bismuth iodide in a molar ratio of 1:1.5 in 0.5 ml of iso-propyl alcohol. This precursor solution is well mixed in a vibrator and is filtered through a 0.45-micron PTFE syringe filter. Then it is coated on top of the electron transport layer at 4000 rpm at 1000 rpm/second for 60 seconds followed by annealing at 110 ^{0}C for 1-5 hours in a nitrogen flow glove box.

c. Bismuth telluride-based

For bismuth telluride-based perovskite, we have to deal with three different materials and coat it to form a single perovskite structure. First layer was bismuth telluride (Bi_2Te_3) (Sigma-Aldrich, 99%) was thermally evaporated in a Cooke Vacuum CV-302-T thermal evaporator with varying thicknesses at a rate of 4-5 Armstrong/second with a chamber pressure of 10^{-5} mbar. Then it was bismuth iodide (BiI_3) (Sigma-Aldrich, 99%), to prepare a precursor solution of bismuth iodide, 200mg of BiI_3 was dissolved in 0.5 ml of dimethylformamide (DMF) as solvent with a volume ratio of 7/3, which was filtered through a 0.45-micron PTFE syringe filter to avoid any undissolved particle. This precursor solution was coated on top of Bi_2Te_3 at 4000 rpm at 1000 rpm/second acceleration for 40 seconds. The substrate was annealed in a nitrogen glove box for 90 minutes at 250^o C.[23] Finally, methylammonium iodide solution was prepared with iso-propyl alcohol at a concentration of 10 mg/ml. This precursor was coated on top of BiI_3 and then annealed for 4-5 hours at 110^o C in a nitrogen glove box. This completes the formation of perovskite structure.

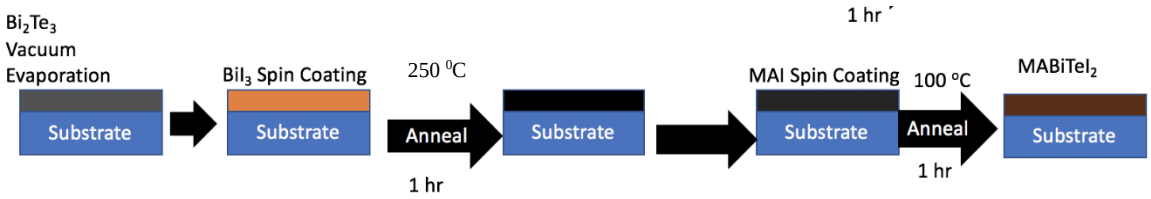

Figure 10: Schematic diagram depicting the three-layer deposition of perovskite

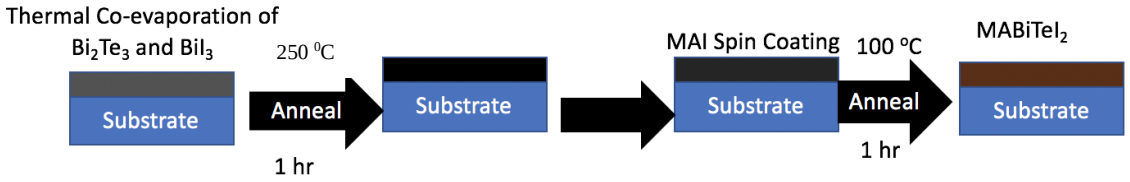

Figure 11: Schematic diagram depicting the deposition of perovskite layer based on thermal co-evaporation

In another method, **thermal co-evaporation** of bismuth iodide (BiI_3) and bismuth telluride (Bi_2Te_3) was conducted. Both the compounds were kept in two different boats in the thermal evaporator, so that the system isn't exposed to the atmosphere before both the layers are coated. A desirable evaporation rate of 4-5 Armstrong/second was used at a chamber pressure of 10^{-5} mbar for the compounds. A series of deposition sequence with varying thicknesses was coated. Some of the sequences are; 20 nm of bismuth telluride (Bi_2Te_3) then 20 nm of bismuth iodide (BiI_3), repeating 3 cycles of the same to attain a thickness of 60 nm of bismuth telluride (Bi_2Te_3) and 60 nm of bismuth iodide (BiI_3). Other sequences were 60 nm of bismuth telluride (Bi_2Te_3) and 60 nm of bismuth iodide (BiI_3) respectively.

2.1.4 Hole transporting layer (HTL)

HTL solution was prepared by dissolving 40 mg of **2,2′,7,7′-Tetrakis[N,N-di(4-methoxyphenyl)amino]-9,9′-spirobifluorene** (Spiro-MeOTAD, Sigma-Aldrich, 99%) in 1ml of chlorobenzene (Sigma-Aldrich, 99.5%), 16 uL of 4-tert-butylpyridine (Sigma-Aldrich, 96%), and 10 uL of lithium salt solution (prepared by dissolving 260 mg of bis(trifluoromethane) sulfonamide lithium salt (Sigma-Aldrich, 99.95%) in 0.5 mL of acetonitrile (Sigma-Aldrich, 99.8%)). The solution was mixed for 10 minutes in a vibrator mixture. The samples were then spin coated with the hole transporting solution at 3000 rpm at 1000 rpm/second for 60 seconds and placed in the desiccator to dry for 24 hours. The exposure of the samples to a dry environment allows the HTM layer to oxidize, increasing conductivity, and thus becoming a better hole transporting material. Until now in all the steps a small piece of tape was placed at the corner with FTO in order to maintain an exposed conductive area during electrical testing.

2.1.5 Metal electrode

Finally, a 100nm thick silver electrode was vacuum evaporated into the sample in a Cooke Vacuum CV-302-T thermal evaporator using metal as mask. A silver deposition rate of 8 angstroms/second was used at a chamber pressure of 10^{-5} mbar. Samples were then stored in a desiccator for 24 hours prior to electrical testing. The total photo-collector area was 0.125 cm^2.

2.2 Characterizations

The current-voltage characteristics of perovskite solar cells were tested by Keithley 2400 source meter which was controlled by the Lab Tracer software. The devices were measured

under forward scanning from -0.3 V to 1 V under dark and then under illumination of 1 sun (which is equivalent to AM 1.5G) from Oriel LCS-100 light source for one minute. The rate at which the measurement was done was 250 mV/s, which corresponds to zero-time delay, and 200 data points were recorded with the voltage range in the Lab Tracer software settings. Current and time were continually recorded during the voltage scan. After forward scanning the devices were forward bias at the applied voltage under illumination. After 1-minute bias, a reverse scanning was done from 1 V to -0.3 V at the same rate and same data points, making it into a reverse bias device. Current and time were recorded for the reverse voltage scan.

The absorption spectra of perovskite thin films were measured by Agilent 8453 UV-Visible spectrophotometer which was controlled by Agilent UV-visible ChemStation software. The thin films were measured for absorbance with a wavelength from 300 nm to 1000 nm.

X-Ray Diffraction measurements were conducted with Philips X'Pert MPD equipped with X'Pert Data Collector. The instrument is first calibrated with quartz SiO_2, which should give a peak at $2\theta = 26.62^o$ with $\pm 0.05^o$. After calibration a suitable program is selected which runs for 5 minutes for 2θ from 5^o to 65^o. If there are visible peaks, then it can be run for 45 minutes for 2θ from 5^o to 65^o for a detailed study of the peaks. Jade 2010 software was used to analyze data.

Energy dispersive spectroscopy measurements were conducted by Jeol 6490-LV equipped with an Oxford Inca X'Act.

CHAPTER 3: Bismuth-based Perovskite Solar Cell

There has been vast research on bismuth-based perovskite solar cell because of the close atomic size between bismuth and lead. However, simply replacing lead with bismuth leads to a different perovskite structure due to the difference in the number of valence electrons. According to Byung-Wood Park [24], the structure of the substances used consists of metal halide octahedra layers and bioctahedral $(Bi_2I_9)^{3-}$ in the form of $A_3B_2X_9$, where A is methylammonium cation (MA^+) (which is a monovalent cation), B is bismuth (Bi) and X is the halide iodide (I).[25] In $(CH_3NH_3)_3Bi_2I_9$ the cluster of $(Bi_2I_9)^{3-}$ bioctahedral structure is surrounded by methylammonium. The power conversion efficiency reported is around 0.12% which is relatively low compared to lead (Pb) based ABX_3 perovskite. Some of the other parameters included the current density, open circuit voltage and fill factor.[26] These parameters are as follows:

$(CH_3NH_3)_3Bi_2I_9$		
J_{sh}	0.52	mA/cm^2
V_{oc}	0.68	V
FF	0.33	
η	0.12	%

Table 1 Bismuth-based perovskite reference parameters

As the first step to develop lead-free perovskites, we also synthesized bismuth-based perovskites using either one-step or two-step method (see details in chapter 2), where bismuth iodide (BiI_3) and methylammonium iodide (CH_3NH_3I) are used as the raw materials. In comparison, the lead-based perovskite $CH_3NH_3PbI_3$ was synthesized with PbI_2 and CH_3NH_3I. The best performed bismuth-based sample fabricated in our laboratory showed the following photovoltaic properties:

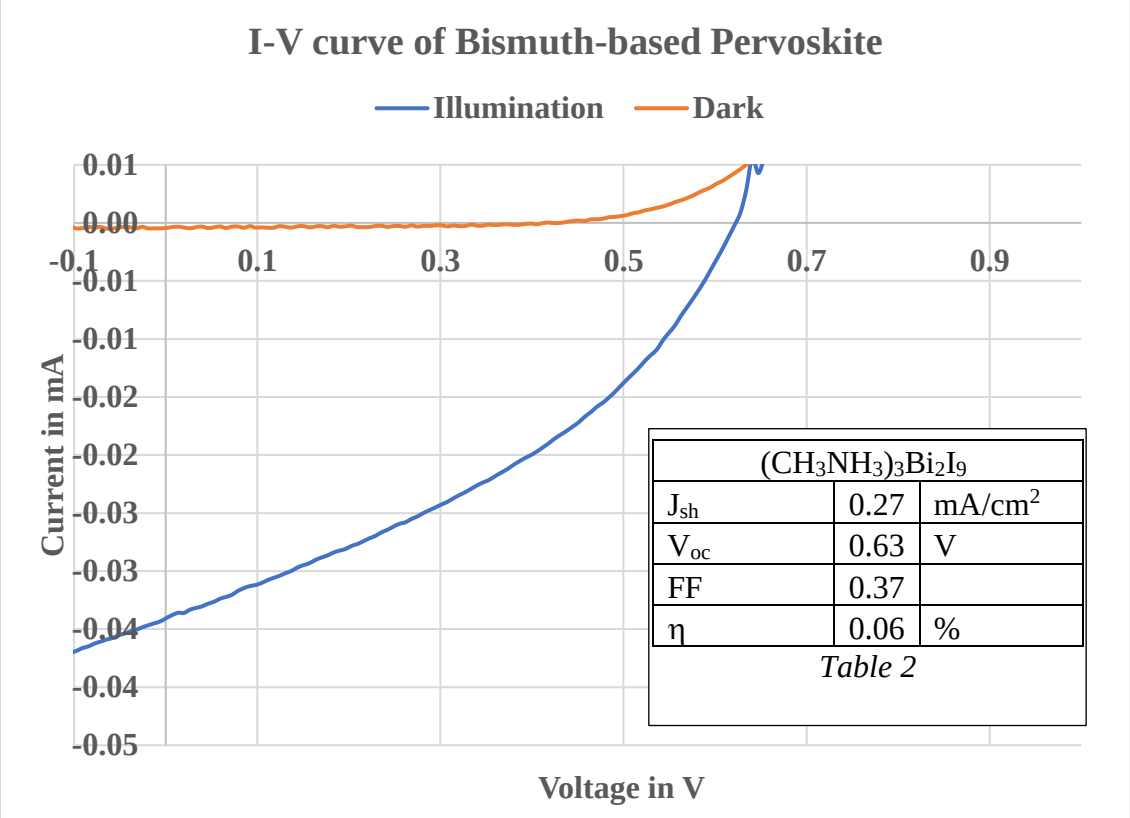

$(CH_3NH_3)_3Bi_2I_9$		
J_{sh}	0.27	mA/cm^2
V_{oc}	0.63	V
FF	0.37	
η	0.06	%

Table 2

Figure 12: I-V characteristic curve of Bismuth-based perovskite

The power conversion efficiency of our sample is just around 5% of the reference[24] However, we see a close comparison in the open circuit voltage and filling factor.[27] There is only 0.05 V difference in the open circuit voltage and 0.04 in the filling factor.

The low short circuit current observed in our solar cells could be attributed to less optimized the working atmosphere and the fabrication control strategies. It could be also related to the weak absorption and low charge mobilities of the $A_3B_2X_9$ perovskite structure.

The absorption spectrum shows a close match with an absorption coefficient of 0.8 x 10^5 cm^{-1} at 450 nm, with the one in reference [24] which estimates the absorption coefficient around 1 x 10^5 cm^{-1} at 450 nm. This is significantly lower when compared with lead-based perovskite ($CH_3NH_3PbI_3$), which is around 2 x 10^5 cm^{-1} at 450 nm.

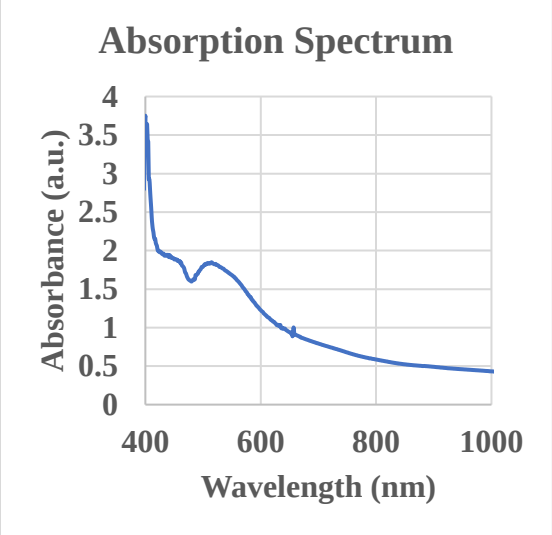

Figure 13: Absorption spectrum of Bismuth based perovskite

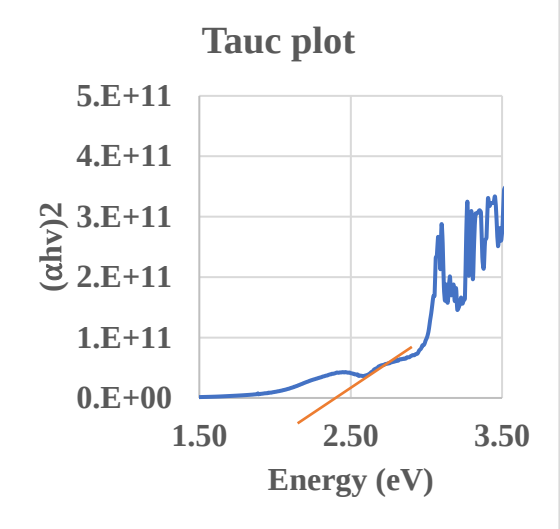

Figure 14: Tauc plot based on absorption spectrum

From the Tauc plot it was found out that the optical bandgap is 2.45 eV, which is close to the calculation based on Byung-Wook Park.[24]

X-ray diffraction was conducted for both one-step and two-step coating methods. As per *figure 15*, it can be noted that there isn't much difference in the two graphs. The only difference is the peak at 24.715^0 for the two-step method perovskite fabrication.

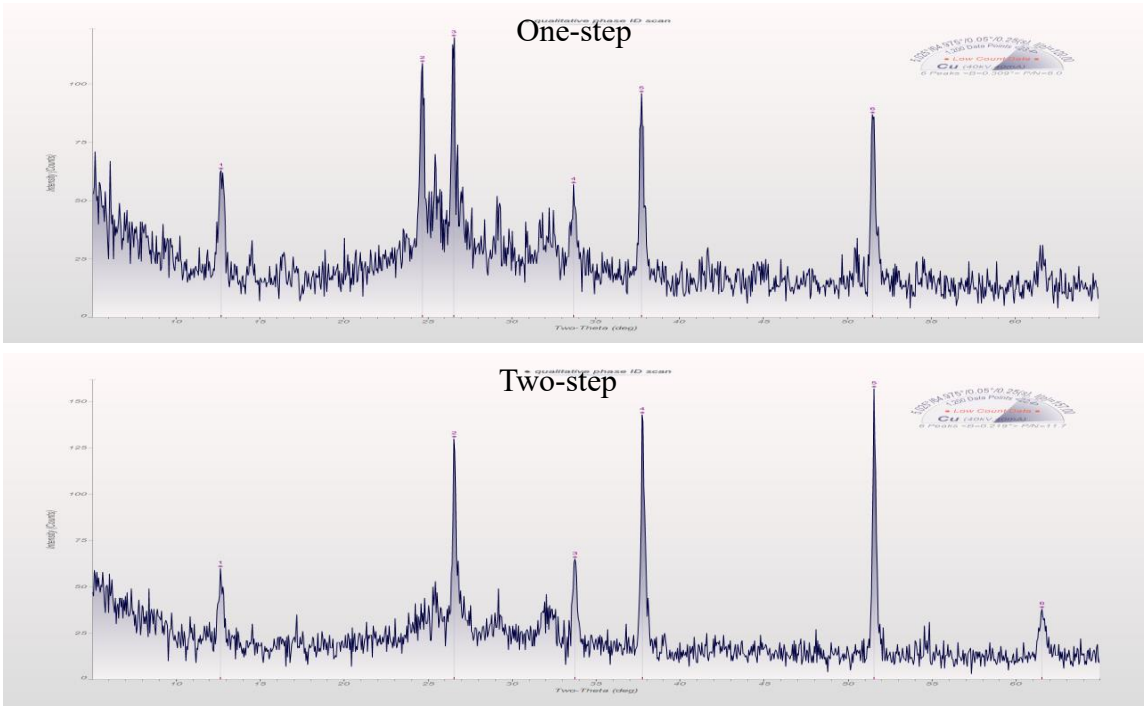

Figure 15: XRD comparison for Bismuth-based one-step and two-step perovskite structures

The X-ray diffraction of one-step method resembles to the reference except the peaks at 37.8 and 51.5^0 for 2θ.[28] This suggests that the structure might be partially formed or might be having defects due to distorted atoms in the process of fabrication. It is also noted that X-ray diffractions for thin films may not always align with the material (powder) itself, this is because, in thin films the structure gets oriented in a particular direction and may not be always perpendicular to the substrate.

In summary, a direct replacement of Pb^{2+} with Bi^{3+} leads to formation $(CH_3NH_3)_3Bi_2I_9$ ($A_3B_2X_9$), which is significantly deviated from the $CH_3NH_3PbI_3$ perovskite structure (ABX_3). The poor photovoltaic performance, especially the extremely low short circuit current, of $(CH_3NH_3)_3Bi_2I_9$ based solar cells indicate the low absorption coefficient and charge mobilities in the $A_3B_2X_9$ structure. It also suggests that it is critical to keep the ABX_3 perovskite structure of $CH_3NH_3PbI_3$ while developing its lead-free alternatives.

CHAPTER 4 Bismuth Telluride-based Perovskite

4.1 Ion-Splitting approach

Replacing lead with another element from the periodic table to perovskite structure has become very difficult to achieve the same optoelectronic properties such as the band gap and charge mobilities. The cation-splitting method works on the basis of splitting a cation into different combinations, like if there are two +2 cations, then they can be split into one 1+ and one 3+ cations. Similarly, if there are two 3+ cations, then they can be split into one 2+ and one 4+ cation. These cation-splitting have been studied and successfully demonstrated by *Shiyou Chen*[29] for kesterite materials. This approach has a greater significance in terms of crystal structure and local chemical environment, as the parent materials are preserved thereby replicating the electronic and optical properties of the desired material. This cation-split method has been a great success in the oxide perovskites and have demonstrated high performing photovoltaic devices.[30] Cation-splitting method has been recently used to explore new perovskite materials in the form of I-II-VII_3 [29].

In a similar way anion-splitting approach could be applied over $CH_3NH_3PbI_3$ to explore lead-free compositions for the perovskite solar cells, as has been proposed in a theoretical research paper.[30]

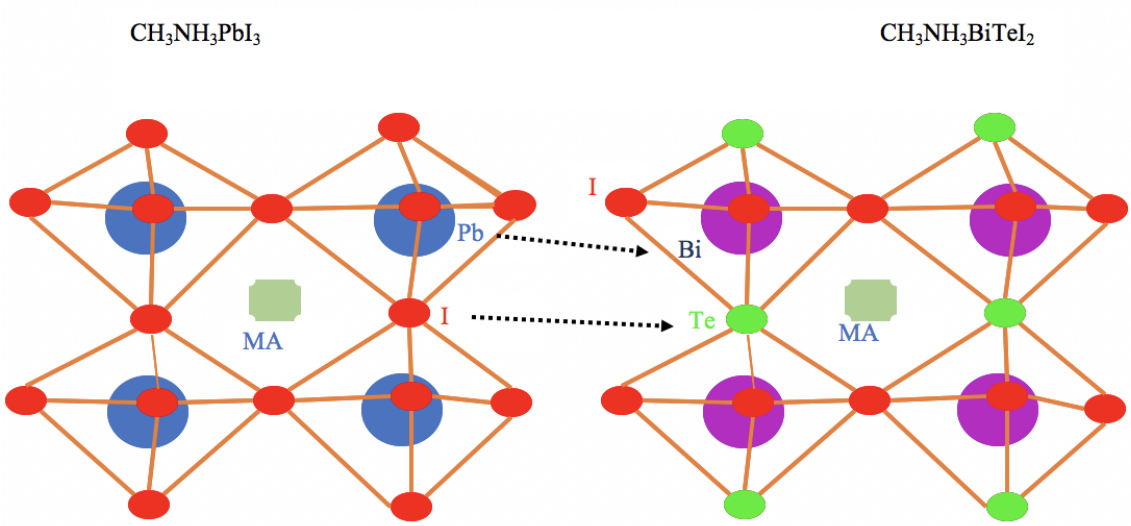

Figure 16: Split-anion approach forming ABX_3 structure [30]

Perovskites with lead in the form of ABX_3 has shown great potential since its discovery. [31]Therefore, it is evident to keep that same structure while developing the lead-free perovskites. The nearest and most suitable element to replace lead in ABX_3 structure would be bismuth (Bi), which is very less in toxicity when compared with lead (Pb), but unfortunately it has a +3 oxidation state. If we simply replace lead (Pb) with bismuth (Bi), as the work shown in chapter 3, it leads to a crystal structure quite different from the ABX_3 perovskite. By applying anion-split method, out of the three iodine (I) per functional unit, it would be split into two iodine (I) and one would be replaced by tellurium into the perovskite core structure, which acts as an acceptor and lead (Pb) being replaced by bismuth (Bi) would maintain charge neutrality. This approach would lead into a compound of I-III-VI-VII_2 structure, where bismuth (Bi) would pair with both group-VI and group-

VII elements. As shown in *figure 16*, the new bismuth telluride perovskite maintains the same crystal structure as the lead-based perovskite.

There are three different approaches to calculate the band gap of the materials. They are: Perdew, Burke and Ernzerhof (PBE), Heyd-Scuseria-Ernzerhof (HSE) and a combination of HSE+ spin-orbit coupling (SOC).[30] The band gap of both $CH_3NH_3PbI_3$ and $CH_3NH_3BiSeI_2$ according to these three calculation methods are listed below:

Band gap in eV			
	PBE	**HSE**	**HSE+SOC**
$CH_3NH_3PbI_3$	**1.57**	**2.52**	**1.54**
$CH_3NH_3BiSeI_2$	**0.94**	**1.81**	**1.29**

Table 3: Band gap with different approaches

The band gap of $CH_3NH_3PbI_3$ as per HSE+SOC rightly aligns with the experimental value of 1.55 eV. Therefore, as per the same calculations based on HSE+SOC we can achieve the band gap for $CH_3NH_3BiSeI_2$ within a close range of 1.28 – 1.30 eV. A series of combination with bismuth (Bi) can be obtained in the form of $CH_3NH_3BiXY_2$ whereby X can be sulfur, selenium or tellurium and Y can be chlorine, bromine or iodine. From these combinations the bandgap was calculated according to HSE+SOC approach by Yi-Yung Sun[30] and they are tabled as follows:

Formulas	Bandgap in eV
$CH_3NH_3BiSCl_2$	2.00
$CH_3NH_3BiSBr_2$	1.68
$CH_3NH_3BiSI_2$	1.38
$CH_3NH_3BiSeCl_2$	1.90
$CH_3NH_3BiSeBr_2$	1.59
$CH_3NH_3BiSeI_2$	1.29
$CH_3NH_3BiTeCl_2$	1.58
$CH_3NH_3BiTeBr_2$	1.44
$CH_3NH_3BiTeI_2$	1.24

Table 4: Calculated band gap for different possible combinations based on HSE+SOC

According to Shockley Queisser theory, the maximum power conversion efficiency for a p-n type solar cell at AM 1.5 solar spectrum is 33.7% which occurs at the bandgap of 1.34 eV. Based on the data shown in *table 4*, it is evident that $CH_3NH_3BiTeI_2$ and $CH_3NH_3BiSeI_2$ are having a bandgap close to the Shockley Queisser theory of 1.34 eV. Furthermore, tellurium has very close ionic radium with iodine, which is another beneficial factor to form the desired crystal structure through ion splitting approach. As such, we decide to move forward with $CH_3NH_3BiTeI_2$ as a target to develop lead-free perovskite for solar cell application.

The lead-free compound of $CH_3NH_3BiTeI_2$ could be formed by mixing bismuth iodide (BiI_3), bismuth telluride (Bi_2Te_3) and methylammonium iodide (CH_3NH_3I). However, bismuth telluride is not soluble in any common solvent. As a result, we proposed a layer-by-layer method to synthesize $CH_3NH_3BiTeI_2$ thin film which is readily incorporated into the solar cell structure shown in *figure 9*. The detailed procedure for the synthesis of $CH_3NH_3BiTeI_2$ and the fabrication of solar cell is shown in chapter 2. In short, a thin film

of bismuth telluride is thermal evaporated on the substrate followed by deposition of bismuth iodide (either through thermal evaporation or spin coating). After annealing and cleaning, another thin film of methylammonium iodide is spin-coated onto the previous layers. And $CH_3NH_3BiTeI_2$ structure will be hopefully formed by annealing the whole sample at an optimized temperature.

4.2 Bismuth Telluride (Bi_2Te_3)-based perovskite and solar cells

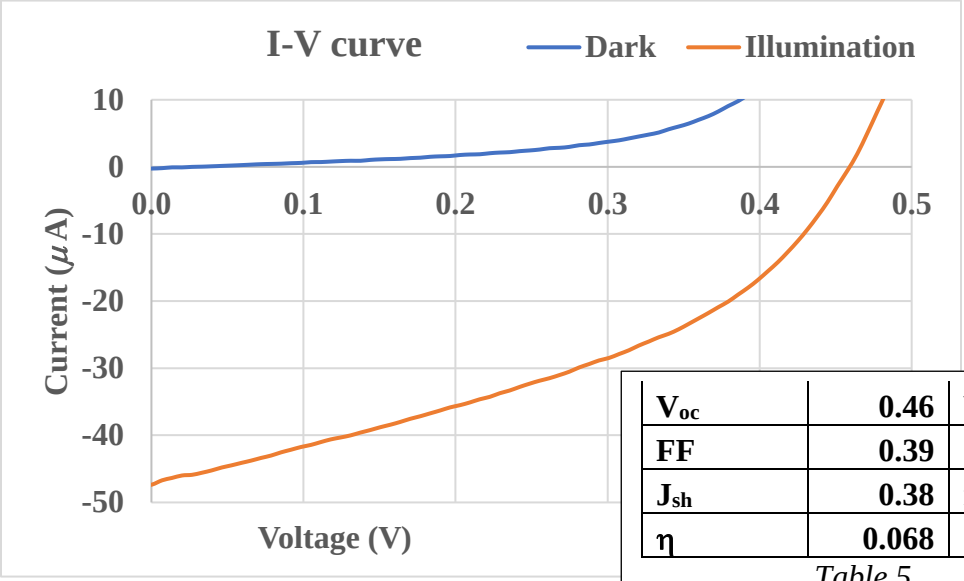

V_{oc}	0.46	V
FF	0.39	
J_{sh}	0.38	mA/cm^2
η	0.068	%

Table 5

Figure 17: I-V characteristics curve of Bismuth telluride-based perovskite solar cell

Upon fabrication (based on chapter 2), the electrical properties were measured and analyzed. The I-V curve in *figure 17* depicts the power conversion efficiency of 0.068% for bismuth telluride-based perovskite solar cell, which is same as that of bismuth-based (as discussed in chapter 3 *Table 2)* perovskite solar cell. However, when we compare other parameters, there is a decrease in the open-circuit voltage from 0.63 V to 0.46 V, a rise in the current density from 0.27 to 0.38 mA/cm^2, whereas there wasn't any change in the fill factor.

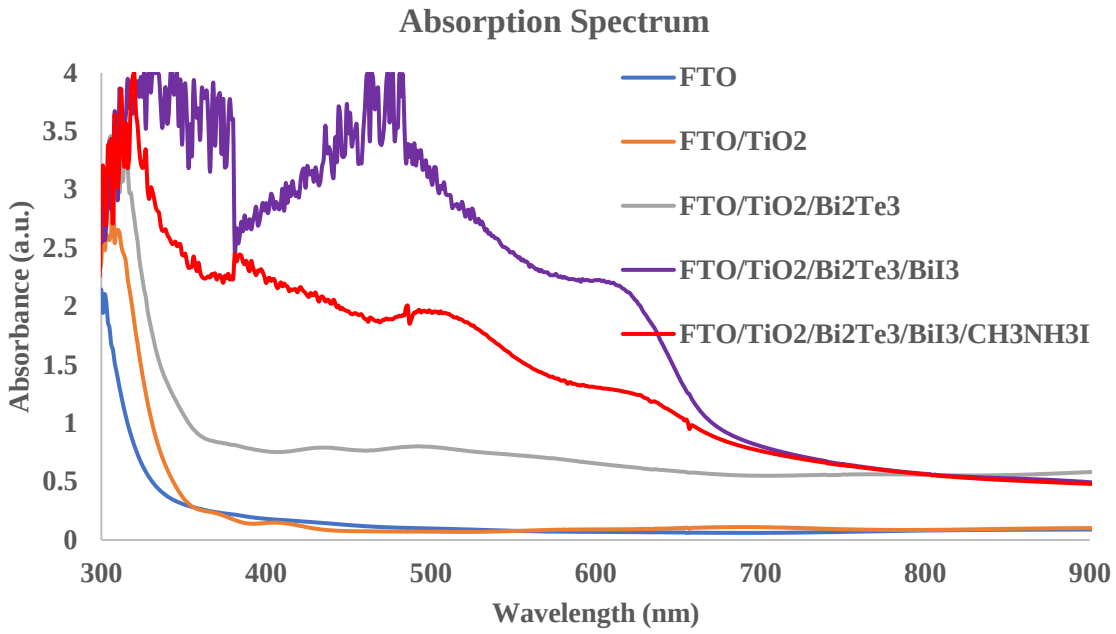

Figure 18: Absorption spectrum after each layer in the fabrication of perovskite solar cell

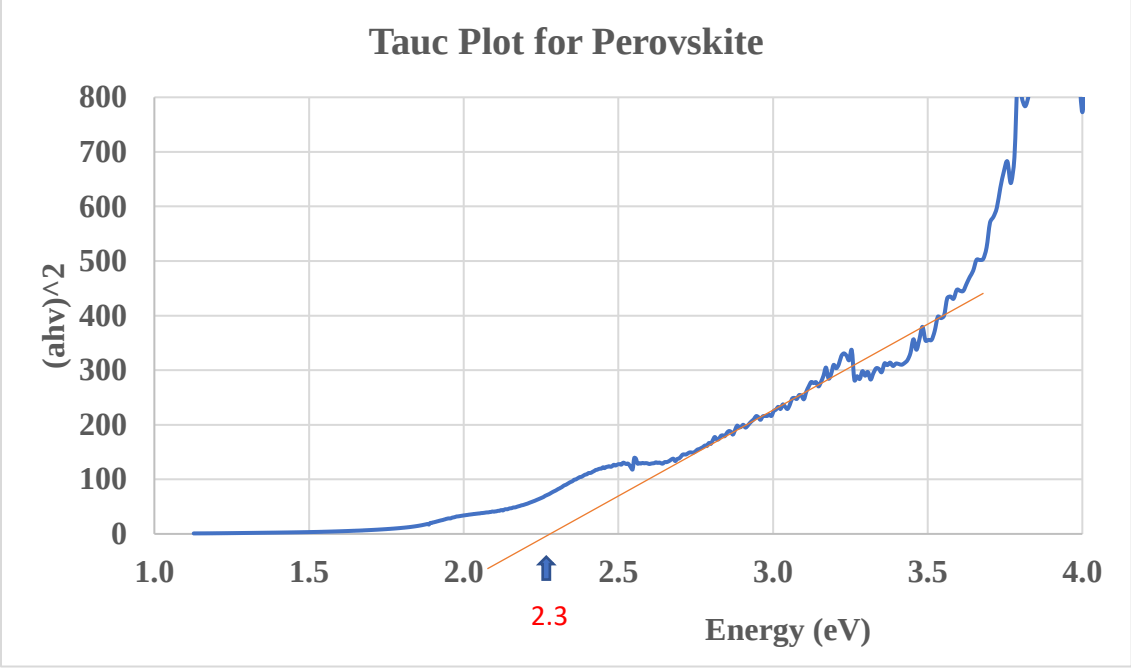

Figure 19: Tauc plot of perovskite layer

F*igure 18* shows the absorption spectrum of different layers starting from the fluorine doped titanium oxide (FTO) to perovskite layer. As we see, the absorbance increases with each layer and its peak shifts toward higher wavelengths. After coating the first layer of the perovskite i.e. bismuth telluride (Bi_2Te_3), there is an increase in the absorbance. Furthermore, when bismuth iodide is coated on top of it, we see a huge shift in the absorbance, as well as there is a huge shift in the peak from a wavelength of 328 nm to 482 nm.[32] Its absorbance range in the wavelength is increasing from 352 nm to until 687 nm i.e. the curve widens, which tells us that there is a greater absorbance for a wide range in the visible spectrum. After the coating of final layer i.e. methylammonium iodide in the perovskite structure, the curve shows a different pattern. The perovskite curve would have raised in a similar fashion as seen with the other layers. However, there is a change in the pattern of the curve which signifies that there is structure forming within the three layers of the perovskite materials. The change of absorption spectra from the double-layer to triple-layer sample is also validated by *figure 20*, where the perovskite structure being coated on the glass substrate.

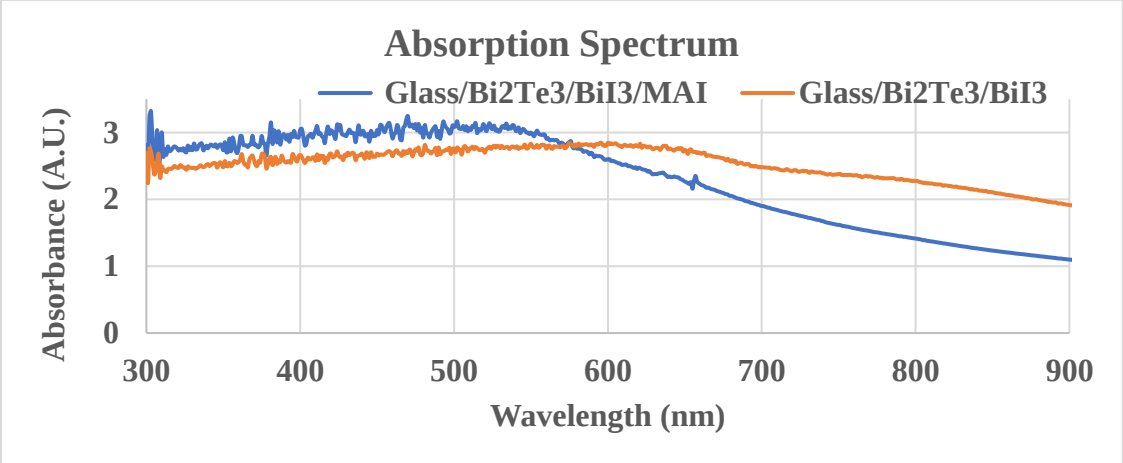

Figure 20: Absorption spectrum of $CH_3NH_3BiTeI_2$ and BiTeI

To study the crystal structure of multi-layer samples, X-ray diffraction measurement were conducted and they gave some insights about the perovskite structure formed.[33]

The first step was to study and analyze the peaks for the film for 2θ where the perovskite structure is formed from a three-step method. Here in *figure 21*, the critical peaks for 2θ at 12.630^0 and 24.715^0 closely resembles to the reference[34], this is with respect to the perovskite formed on titanium oxide (TiO_2) substrate.

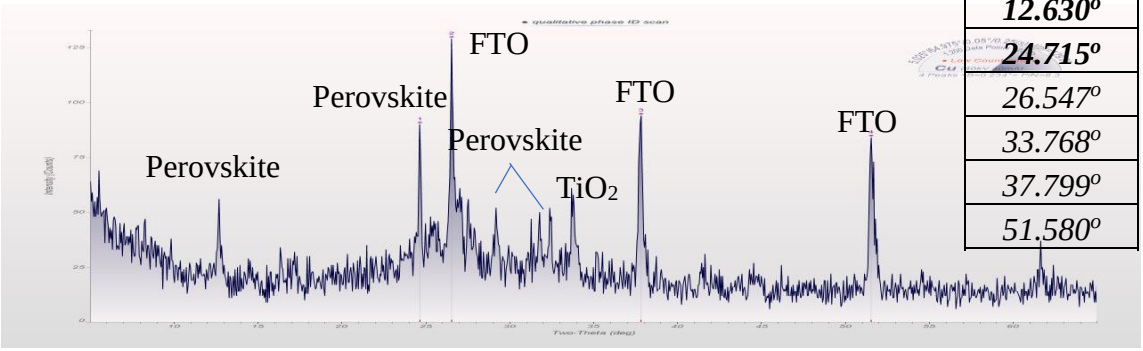

2θ
12.630º
24.715º
26.547º
33.768º
37.799º
51.580º

Figure 21: XRD of Bismuth telluride-based perovskite solar cell

Also, *figure 21* shows similar peaks with that of $(CH_3NH_3)_3Bi_2I_9$. However, with two- step fabrication method shown in *figure 15* there isn't any peak for 2θ at 24.715^0. This partially tells us that bismuth (Bi) in bismuth telluride (Bi_2Te_3) is partially reacting and forming a structure similar to $(CH_3NH_3)_3Bi_2I_9$.

As the perovskites were deposited on titanium oxide layer (TiO_2), which plays a very vital role in providing a platform for the perovskite structure to form. The mesoporous structure of TiO_2 provides a continuous particle framework, high surface area, nanocrystallinity and scaffolding base for the lead-based perovskite structure. [35] In our study, the X-ray diffractions for perovskites on glass substrate didn't show any reasonable peaks which

suggests an amorphous structure. Similar results have been reported, for example, research done by *A. Hosseini* on TiO_2 structure revealed that the structure is amorphous on glass substrate whereas it is crystalline in nature when coated on FTO substrate.[36]

4.3 Optimization of annealing temperatures

In a three-step layer-by-layer synthesis, the thin film samples consisting of Bi_2Te_3 and BiI_3 have to be annealed to form the BiTeI octahedral structure as shown in *Figure 8*, then after the third layer, CH_3NH_3I, was deposited the samples will be further annealed to form $CH_3NH_3BiTeI_2$ perovskite structure. The absorption spectra of Bi_2Te_3/BiI_3 double-layer sample at different annealing temperatures are shown in *figure 22*, which presents that the sample without annealing exhibits a broad absorption at visible range with multiple peaks, while the sample annealed above 200 ^oC shows a single peak at around 600nm. The shifting of absorption peak can be visibly observed as sample's color change. At 250 ^0C, we see complete peak shifting and the strongest absorption intensity at peak position, suggesting a complete conversion of Bi_2Te_3/BiI_3 to BiTeI. As a result, the annealing temperature for Bi_2Te_3/BiI_3 double-layer is control at around 250 ^0C. *Figure 23* shows the absorption spectra for triple-layer samples at different annealing temperature. The absorption spectrum of the sample annealed at 120 ^0C displays multiple peaks that could be related to $CH_3NH_3BiTeI_2$. However, those peaks disappeared when the annealing temperature was increased to 180 ^0C. It is known that the hybrid perovskite $CH_3NH_3PbI_3$ is not thermally stable, and it decomposes at relatively high temperature[39]. The disappearance of absorption peaks at 180 ^oC suggests $CH_3NH_3BiTeI_2$ may have the same thermal stability

issue. Annealing the perovskite structure at 180^0 C may decompose methylammonium and thereby leaving behind a non-stoichiometry mixture of bismuth, iodide and telluride. [40][41] As a result, the annealing temperature for the triple-layer samples has to be controlled below 120 ^{0}C.

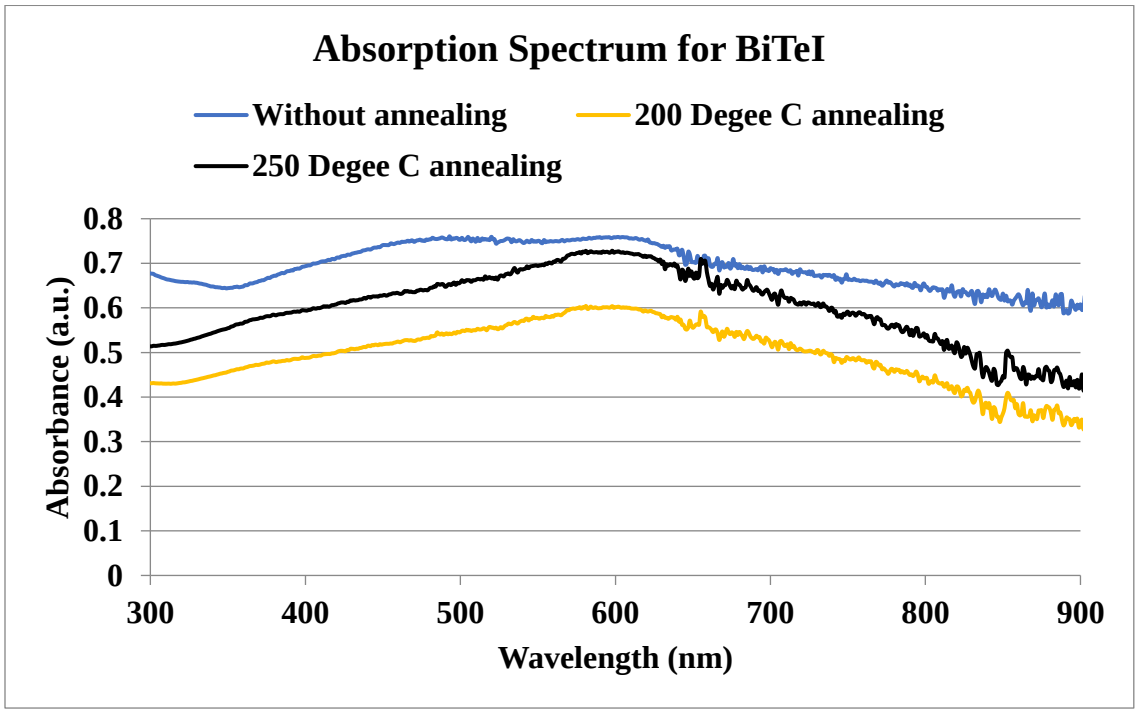

Figure 22: Absorption Spectrum for the annealing effect of BiTeI

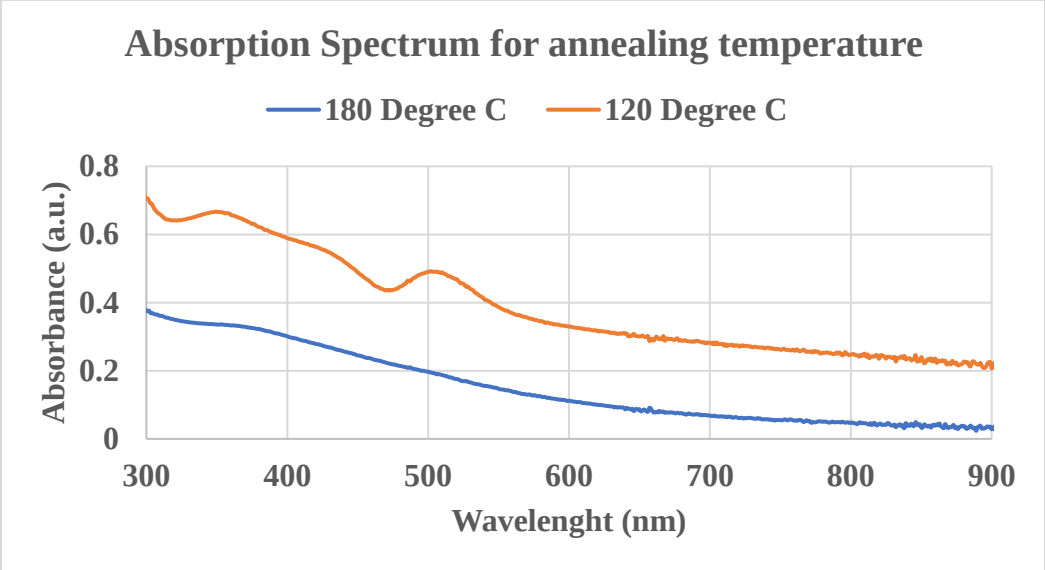

Figure 23: Annealing temperatures for bismuth telluride-based perovskite

4.4 Physical Vapor Deposition of Bismuth Telluride (Bi_2Te_3)

The physical vapor deposition **Bismuth Telluride (Bi_2Te_3)** plays a major role in the formation of perovskite structure in our process. Since Bi_2Te_3 is insoluble in most solvents, it cannot be deposited by solution-based spin coating. Some of the techniques for depositing Bi_2Te_3 for thin films are co-sputtering, electrochemical deposition, metal-organic chemical vapor deposition and flash evaporation. [43]Thermal evaporation is one of the simple and attractive techniques to coat insoluble compounds. However, the works done by L.M. Goncalves [43] showed that due to the huge difference in the partial vapor pressure of bismuth and telluride, there is a compositional gradient difference in the deposited films. Therefore, the thermally evaporated bismuth telluride (Bi_2Te_3) would be Bi_xTe_y, whereby the values of x and y may vary depending on the rate of evaporation, film thickness and annealing temperature. Considering the facts, the films demonstrated can be

in the form of $CH_3NH_3Bi_xTe_yI_z$, where even the composition of iodide (I) can't be determined. It is shown in earlier research[33], that the films coated by sputtering (which is one of the methods of physical vapor deposition method) resulted in a Te-rich film and when the films where annealed it showed a reduction of Te in the film. With the rise in the annealing temperature, Te evaporates from the film. After a certain temperature i.e. at more than 300^0 C bismuth telluride (Bi_2Te_3) is reduced down to BiTe, which is a completely different structure and thereby it changes its properties. Therefore, our research, the annealing temperature is controlled at/below 250 ^oC, so as to maintain the stoichiometry and to form a reaction with bismuth iodide and form BiTeI.

Further in another reference, a composition rich in bismuth was studied, based on thermal evaporation. [45] In this study, Bi_2Te_3 becomes a p-type material, this is because the anti-site defects of tellurium lattice sites are being occupied by bismuth. This extreme non-stoichiometry defect is the cause of the charge carrier concentration resulting from the anti-site defects. This is one of the demerits of the coating methods in thermal evaporation. If the compound is evaporated a higher rate, then it will have more energy, which might cause a tendency of bismuth sticking into the substrate and the tellurium atoms may get reflected from the substrate and will make a low concentrated tellurium or tellurium deficiency in the film.[46] As a result, co-evaporating bismuth and tellurium from two separate sources would be more viable approach to form bismuth telluride (Bi_2Te_3) with a desired composition.[48]

To verify the chemical compositions in thermal evaporated bismuth telluride (Bi_2Te_3) thin films in our research, energy dispersive X-ray spectroscopy (EDS) measurements were conducted on both bismuth telluride powder and thin films.

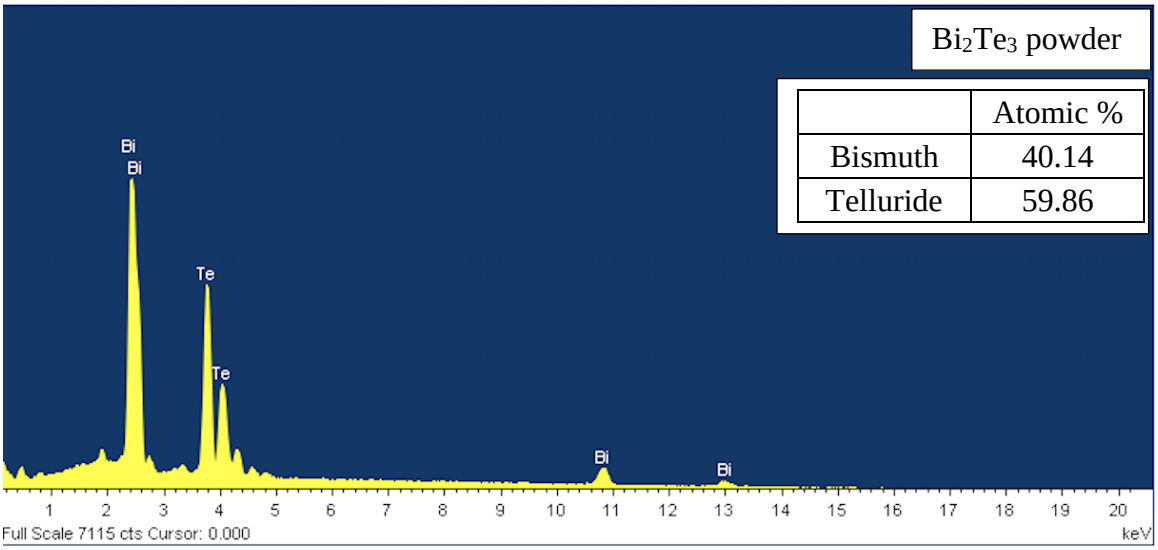

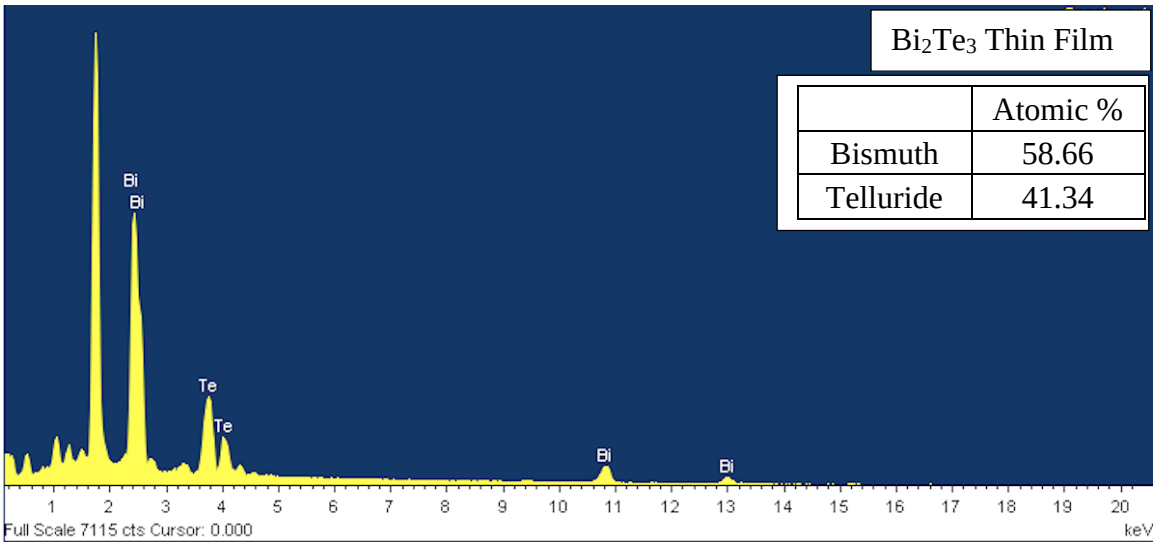

Figure 24: Energy dispersive spectrum of Bi_2Te_3 powder and a thermal evaporated Bi_2Te_3 thin film

In *figure 24* we see the clear difference in the composition, where the atomic percentage of bismuth and telluride are approximately 40 and 60 % in the powder, whereas in thin films it is just the opposite which is 60 % bismuth and 40 % telluride. The composition varies with the deposition parameters such as deposition rate and substrate temperature. Nonetheless, the result aligns with the references and suggests thermal evaporation will most likely produce nonstoichiometric bismuth telluride thin films.[49][50]

In summary, a three-layer deposition method was adopted to fabricate a lead-free perovskite $CH_3NH_3BiTeI_2$, which resembles the ABX_3 structure in lead-based perovskites. The solar cells fabricated based on $CH_3NH_3BiTeI_2$ showed a power conversion efficiency of 0.06% including a current density of 0.38 mA/cm^2 and open-circuit voltage of 0.46 V. Absorption spectra and X-ray diffraction reveal partial conversion of the triple-layer sample to the ABX_3 structure. The incomplete conversion to the desired perovskite structure is attributed to the nonstoichiometric bismuth telluride thin films deposited by thermal evaporation.

CHAPTER 5 Conclusion and Future Scope

In recent years with the discovery of perovskite structure there has been a boom in the research of perovskite solar cells. These perovskites contain lead (Pb) which is not environmentally friendly. Lots of research have been done to develop lead (Pb)-free perovskite structure for solar cell application.

There are various lead (Pb)-free perovskites being studied and researched, but none of it have reached even close to it when compared with the properties like power conversion efficiency (PCE) as that of $CH_3NH_3PbI_3$. The tetragonal structure of lead (Pb)-based perovskite plays a very vital role in obtaining these properties. As discussed in chapter 4, anion-spilt approach with bismuth telluride (Bi_2Te_3) would possibly give a tetragonal structure as that of lead (Pb) based perovskite solar cell, which can be attributed as novelty of this research including the experimental setup which consists of the fabrication of $CH_3NH_3BiTeI_2$ perovskite solar cell.

In this study, a three-layer deposition method to form a lead-free perovskite $CH_3NH_3BiTeI_2$ was formulated and this holds first of its kind to proceed at an experimental level. Specifically, first bismuth telluride (Bi_2Te_3) was thermal evaporated, after that bismuth iodide (BiI_3) was solvent coated and was annealed to facilitate reaction between these two layers to form BiTeI. Finally, methylammonium iodide (CH_3NH_3I) was solvent coated and annealed, so that all the three layers would form a single $CH_3NH_3BiTeI_2$ structure. The solar cells fabricated based on $CH_3NH_3BiTeI_2$ showed a power conversion efficiency of 0.06% including a current density of 0.38 mA/cm^2 and open-circuit voltage of 0.46 V.

Absorption spectrum revealed the formation of a new structure within these three layers. X-ray diffraction reveals amorphous structure for the films coated on a glass substrate, while the samples coated on TiO_2 substrates (which is the electron transporting layer of the solar cell) showed a few diffraction peaks matching with the tetragonal structure of $MAPbI_3$, suggesting the desired perovskite structure is partially formed. The incomplete conversion of the desired $CH_3NH_3BiTeI_2$ perovskite structure is attributed to the nonstoichiometric bismuth telluride thin films deposited by thermal evaporation.

Therefore, thermal evaporation of bismuth telluride (Bi_2Te_3) is to be optimized so as to avoid the compositional gradient[43]. To completely avoid this difference in the compositional gradient and formation of distorted compound, thermal co-evaporation of bismuth (Bi) and telluride (Te) can be done separately as suggested by L.M. Goncalves[43]. The physical vapor deposition should be done at different rates to ensure controlled deposition, thereby attaining an accurate composition of Bi_2Te_3. While in this study a specific experimental procedure was followed, new experimental techniques and models can be adopted for the improvement of each measurement and model used.

Mesoporous TiO_2 substrate was found to facilitate the formation of lead-free perovskite structure which is consistent with the reported research on lead-based perovskites.[36] Therefore, it would be interesting to further investigate the effect of TiO_2, e.g. the size TiO_2 nanoparticles and thickness of mesoporous layer on the lead-free perovskite structure formation kinetics.

References

[1] "BP Statistical Review of World Energy Statistical Review of World," 2019.

[2] J. Tsao, N. Lewis, and G. Crabtree, "Solar FAQs," *US Dep. Energy*, pp. 1–24, 2006.

[3] R. Fu, D. Feldman, and R. Margolis, "U.S. Solar Photovoltaic System Cost Benchmark: Q1 2018," *Nrel*, no. Novmnber, pp. 1–47, 2018.

[4] N. Park, *Organic- Inorganic Halide Perovskite Photovoltaics*. .

[5] US National Renewable Energy Laboratory, "Best Research-Cell Efficiencies," *Nrel*. p. 1, 2019.

[6] D. K. Bhattacharya, "DEVICES."

[7] D. K. Bhattacharya, "Energy Bands and Charge," *Solid state Electron. devices*, pp. 65–122, 2013.

[8] O. Devices, "Opto-electronic Devices."

[9] A. H. M. Smets, K. Jäger, O. Isabella, R. A. van Swaaij, and M. Zeman, "Solar Cell Parameters and Equivalent Circuit," *Sol. energy Phys. Eng. Photovolt. conversion, Technol. Syst.*, pp. 113–121, 2016.

[10] W. A. Harrison, "Electron Dynamics," *Appl. Quantum Mech.*, pp. 189–196, 2013.

[11] A. Kojima, K. Teshima, Y. Shirai, and T. Miyasaka, "Organometal halide perovskites as visible-light sensitizers for photovoltaic cells," *J. Am. Chem. Soc.*, vol. 131, no. 17, pp. 6050–6051, 2009.

[12] Y. Yan, W. J. Yin, T. Shi, W. Meng, and C. Feng, *Defect physics of CH3NH3PbX3 (X=I, Br, Cl) perovskites*. 2016.

[13] T. Oku, "Crystal Structures of CH3NH3PbI3 and Related Perovskite Compounds Used for Solar Cells," *Sol. Cells - New Approaches Rev.*, 2015.

[14] N. G. Park, M. Grätzel, T. Miyasaka, K. Zhu, and K. Emery, "Towards stable and commercially available perovskite solar cells," *Nat. Energy*, vol. 1, no. 11, 2016.

[15] N. G. Park, "Perovskite solar cells: An emerging photovoltaic technology," *Mater. Today*, vol. 18, no. 2, pp. 65–72, 2015.

[16] A. Abate, "Perovskite Solar Cells Go Lead Free," *Joule*, vol. 1, no. 4, pp. 659–664, 2017.

[17] R. Ali, G. J. Hou, Z. G. Zhu, Q. B. Yan, Q. R. Zheng, and G. Su, "Predicted Lead-Free Perovskites for Solar Cells," *Chem. Mater.*, vol. 30, no. 3, pp. 718–728, 2018.

[18] Z. Zhao *et al.*, “Mixed-Organic-Cation Tin Iodide for Lead-Free Perovskite Solar Cells with an Efficiency of 8.12%,” *Adv. Sci.*, vol. 4, no. 11, 2017.

[19] H. S. Jung and N. G. Park, “Perovskite solar cells: From materials to devices,” *Small*, vol. 11, no. 1, pp. 10–25, 2015.

[20] L. Liang and P. Gao, “Lead-Free Hybrid Perovskite Absorbers for Viable Application: Can We Eat the Cake and Have It too?,” *Adv. Sci.*, vol. 5, no. 2, 2018.

[21] “Spin Speed,” *Coating*.

[22] “Mesoporous Titanium Dioxide.pdf.” .

[23] A. Kulkarni, T. Singh, A. K. Jena, P. Pinpithak, M. Ikegami, and T. Miyasaka, “Vapor Annealing Controlled Crystal Growth and Photovoltaic Performance of Bismuth Triiodide Embedded in Mesostructured Configurations,” *ACS Appl. Mater. Interfaces*, vol. 10, no. 11, pp. 9547–9554, 2018.

[24] “Bismuth based Perovskite solar cell.pdf.” .

[25] “methylammonium bismuth iodide.pdf.” .

[26] Z. Zhang *et al.*, “ High-Quality (CH 3 NH 3) 3 Bi 2 I 9 Film-Based Solar Cells: Pushing Efficiency up to 1.64% ,” *J. Phys. Chem. Lett.*, vol. 8, no. 17, pp. 4300–4307, 2017.

[27] M. Lyu *et al.*, “Organic–inorganic bismuth (III)-based material: A lead-free, air-stable and solution-processable light-absorber beyond organolead perovskites,” *Nano Res.*, vol. 9, no. 3, pp. 692–702, 2016.

[28] V. Bulovic, “Supporting Information Methylammonium Bismuth Iodide as a Lead-Free , Stable Hybrid Organic – Inorganic Solar Absorber.”

[29] S. Chen, X. G. Gong, A. Walsh, and S. H. Wei, “Crystal and electronic band structure of Cu2 ZnSn X4 (X=S and Se) photovoltaic absorbers: First-principles insights,” *Appl. Phys. Lett.*, vol. 94, no. 4, pp. 94–97, 2009.

[30] Y. Y. Sun *et al.*, “Discovering lead-free perovskite solar materials with a split-anion approach,” *Nanoscale*, vol. 8, no. 12, pp. 6284–6289, 2016.

[31] F. Sani, S. Shafie, H. N. Lim, and A. O. Musa, “Advancement on lead-free organic-inorganic

halide perovskite solar cells: A review," *Materials (Basel).*, vol. 11, no. 6, pp. 1–17, 2018.

[32] Z. Xiao, Y. Zhou, H. Hosono, T. Kamiya, and N. P. Padture, "Bandgap Optimization of Perovskite Semiconductors for Photovoltaic Applications," *Chem. - A Eur. J.*, vol. 24, no. 10, pp. 2305–2316, 2018.

[33] K. Singkaselit, A. Sakulkalavek, and R. Sakdanuphab, "Effects of annealing temperature on the structural, mechanical and electrical properties of flexible bismuth telluride thin films prepared by high-pressure RF magnetron sputtering," *Adv. Nat. Sci. Nanosci. Nanotechnol.*, vol. 8, no. 3, 2017.

[34] Z. Ren *et al.*, "Thermal assisted oxygen annealing for high efficiency planar CH3NH3PbI3 perovskite solar cells," *Sci. Rep.*, vol. 4, no. October, 2014.

[35] A. K. Jena, H. W. Chen, A. Kogo, Y. Sanehira, M. Ikegami, and T. Miyasaka, "The interface between FTO and the TiO<inf>2</inf> compact layer can be one of the origins to hysteresis in planar heterojunction perovskite solar cells," *ACS Appl. Mater. Interfaces*, vol. 7, no. 18, pp. 9817–9823, 2015.

[36] A. Hosseini, K. Içli, M. Özenbaş, and Erçelebi, "Fabrication and characterization of spin-coated TiO2films," *Energy Procedia*, vol. 60, no. C, pp. 191–198, 2014.

[37] C. Ran *et al.*, "Construction of Compact Methylammonium Bismuth Iodide Film Promoting Lead-Free Inverted Planar Heterojunction Organohalide Solar Cells with Open-Circuit Voltage over 0.8 V," *J. Phys. Chem. Lett.*, vol. 8, no. 2, pp. 394–400, 2017.

[38] S. Guo, K. Hayakawa, and C. Link, "(Article begins on next page)," *Diabetes*, vol. 60, no. 8, pp. 1789–1796, 2016.

[39] J. C. Hebig, I. Kühn, J. Flohre, and T. Kirchartz, "Optoelectronic Properties of (CH3NH3)3Sb2I9 Thin Films for Photovoltaic Applications," *ACS Energy Lett.*, vol. 1, no. 1, pp. 309–314, 2016.

[40] S. Sanders *et al.*, "Chemical Vapor Deposition of Organic-Inorganic Bismuth-Based Perovskite Films for Solar Cell Application," *Sci. Rep.*, vol. 9, no. 1, pp. 1–8, 2019.

[41] M.-C. Tang *et al.*, "Bismuth-Based Perovskite-Inspired Solar Cells: In Situ Diagnostics Reveal Similarities and Differences in the Film Formation of Bismuth- and Lead-Based Films," *Sol. RRL*, vol. 3, no. 7, p. 1800305, 2019.

[42] S. Worasukhkhung, S. Pudwat, P. Eiamchai, M. Horprathum, S. Dumrongrattana, and K. Aiempanakit, “Hydrophilic property of TiO2 films sputtered on glass/ITO for self cleaning glass and heat mirror application,” *Procedia Eng.*, vol. 32, pp. 780–786, 2012.

[43] L. M. Goncalves, C. Couto, P. Alpuim, A. G. Rolo, F. Völklein, and J. H. Correia, “Optimization of thermoelectric properties on Bi2Te3 thin films deposited by thermal co-evaporation,” *Thin Solid Films*, vol. 518, no. 10, pp. 2816–2821, 2010.

[44] L. M. Gonçalves, J. G. Rocha, J. H. Correia, and C. Couto, “Control of the deposition ratio of Bi2Te3 and Sb 2Te3 in a vacuum evaporator for fabrication of Peltier elements,” *IEEE Int. Symp. Ind. Electron.*, vol. 4, pp. 2773–2777, 2006.

[45] D. Physique, E. Mines, P. De Sanrupt, and N. Cedex, “Thermal Properties of high quality Bismuth Telluride,” no. 10, pp. 1–11, 2011.

[46] W. Lu, Y. Ding, Y. Chen, Z. L. Wang, and J. Fang, “Bismuth telluride hexagonal nanoplatelets and their two-step epitaxial growth,” *J. Am. Chem. Soc.*, vol. 127, no. 28, pp. 10112–10116, 2005.

[47] A. T. Devoe, A. Prof, and S. Oh, “Properties of RF Sputter Deposited Bismuth Telluride Thin Films List of Figures,” pp. 1–9.

[48] J. Dheepa, R. Sathyamoorthy, S. Velumani, A. Subbarayan, K. Natarajan, and P. J. Sebastian, “Electrical resistivity of thermally evaporated bismuth telluride thin films,” *Sol. Energy Mater. Sol. Cells*, vol. 81, no. 3, pp. 305–312, 2004.

[49] C. V. Manzano *et al.*, “Thermoelectric properties of Bi2Te3 films by constant and pulsed electrodeposition,” *J. Solid State Electrochem.*, vol. 17, no. 7, pp. 2071–2078, 2013.

[50] K. Park *et al.*, “Extraordinary Off-Stoichiometric Bismuth Telluride for Enhanced n-Type Thermoelectric Power Factor,” *J. Am. Chem. Soc.*, vol. 138, no. 43, pp. 14458–14468, 2016.

[51] Ball, J.M.; Lee, M.M.; Hey, A.; Snaith, H.J. Low-temperature processed meso-superstructured to thin-film perovskite solar cells. Energy Environ. Sci. 2013, 6, 1739–1743. [CrossRef]

[52] Stoumpos, C.C.; Malliakas, C.D.; Kanatzidis, M.G. Semiconducting tin and lead iodide perovskites with organic cations: Phase transitions, high mobilities, and near-infrared photoluminescent properties. Inorg. Chem. 2013, 52, 9019–9038. [CrossRef]

[53] Im, J.H.; Lee, C.R.; Lee, J.W.; Park, S.W.; Park, N.G. 6.5% efficient perovskite quantum-dot-sensitized solar cell. Nanoscale 2011, 3, 4088–4093. [CrossRef] [PubMed]

[54] World Energy Balances statistics 2019, International Energy Agency

Appendix A Laboratory Safety

It is important to maintain certain laboratory safety standards while fabrication the samples as well as while testing them in certain conditions. A minimum laboratory safety standard includes:

1. Awareness of the physical and chemical properties of laboratory reagents being used and of the safety and health hazards they pose
2. Availability and use of proper apparatus and control infrastructure to carry out procedures safely
3. Knowledge and application of additional special practices necessary to reduce risks
4. Familiarity and skill with emergency prodedures
5. Well designed and organised workspace that facilitates safe operation, protects workers from hazardous environments, allows unrestricted movement about the laboratory, and allows for the segregation of hazards
6. Use of proper personal protective equipment

Before starting any laboratory work, a research safety training is completed, which was designed by the Department of Environmental Health and Safety, University of Minnesoata. This training eqips with the basic handling of chemicals and laboratory equipments. Also, it imparts with the safety measures in the laboratory.

All chemical solvent transfer was done in fume hood. Personal protective equipments like safety glasses, laboratory apron, gloves and shoes were used all the time in the laboratory. Sharp needles and fabricated samples were disposed safely in the designated

disposal container. The disposal of sample test tube containers and pipette tips were done with proper disposal procedures as they contained the solvents and chemicals being used in the fabrication process of perovskite solar cell. None of the solvents or chemicals are flushed or dumped in the sink.

X-Ray

Special training is needed for the access and operation of Philips X'Pert MPD. Some of the basic safety standards of X-ray are:

1. minimizing time around a radiation source will reduce total exposure
2. maximizing the distance from a radiation source to reduce the total exposure
3. shielding materials reduce occupational exposure

Some of the sources of exposure are from primary beam, diffracted rays from crystals, secondary emission from sample or shielding material, leakage from primary beam through cracks in shielding, penetration of primary beam through shutters, cameras, etc. A SOP formulated by the Research Instrumentation Laboratory (RIL) at the University of Minnesota Duluth, was followed as a safety precaution.

Supporting Materials:

Few images being taken for reference are:

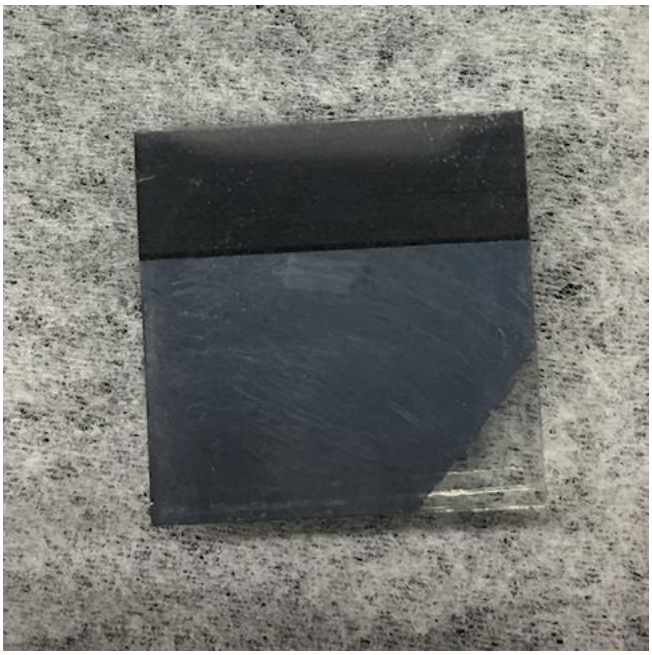

Figure S1: Bi_2Te_3 50 nm film

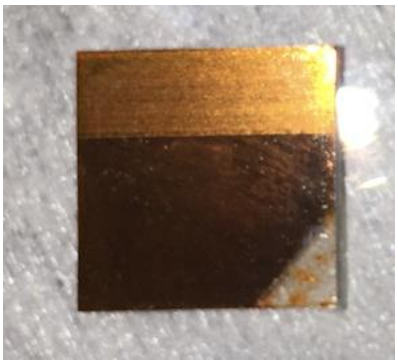

Figure S2: BiTeI film before annealing

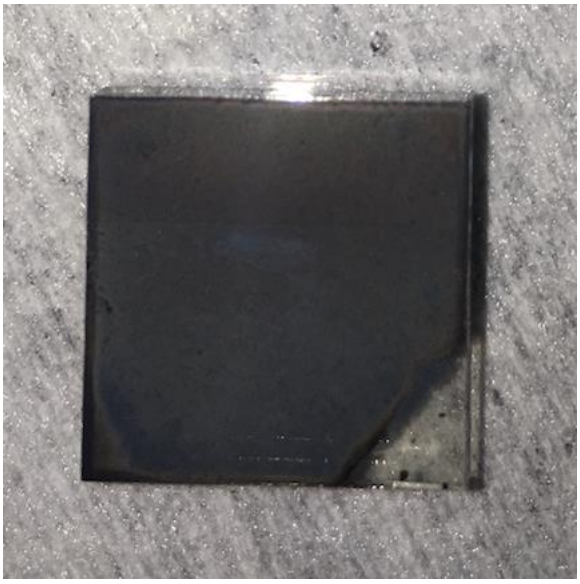

Figure S3: BiTeI film after annealing

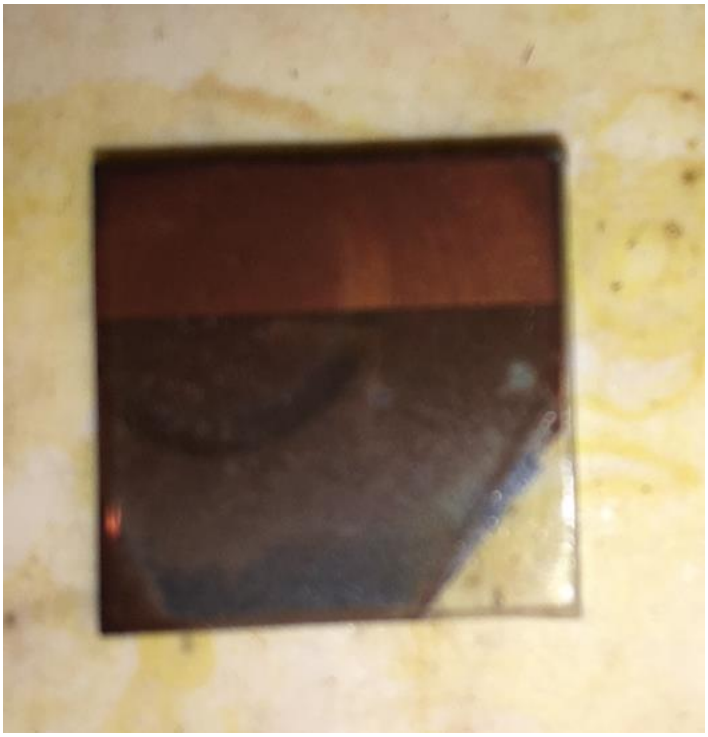

Figure S4: Perovskite film $CH_3NH_3BiTeI_2$